AGU PUBLICATIONS

Geochemistry, Geophysics, Geosystems

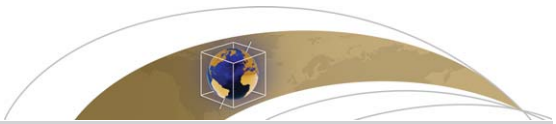

RESEARCH ARTICLE

10.1002/2014GC005514

Key Points:
- Controls on B/Ca ratios in shells of *Globigerinoides ruber* are investigated
- Strong carbonate system effects are seen in culture, supporting previous work
- In the open ocean, however, $[PO_4^{3-}]$ and (to a lesser extent) salinity appear to be the primary controls

Supporting Information:
- Supporting Information S1

Corresponding To:
M. J. Henehan, mailto:
Michael.Henehan@yale.edu

Citation:
Henehan, M. J., G. L. Foster, J. W. B. Rae, K. C. Prentice, J. Erez, H. C. Bostock, B. J. Marshall, and P. A. Wilson (2015), Evaluating the utility of B/Ca ratios in planktic foraminifera as a proxy for the carbonate system: A case study of *Globigerinoides ruber*, *Geochem. Geophys. Geosyst.*, *16*, 1052–1069, doi:10.1002/2014GC005514.

Received 22 JUL 2014
Accepted 6 MAR 2015
Accepted article online 13 MAR 2015
Published online 4 APR 2015

The copyright line for this article was changed on 14 MAY 2015 after original online publication.

Evaluating the utility of B/Ca ratios in planktic foraminifera as a proxy for the carbonate system: A case study of *Globigerinoides ruber*

Michael J. Henehan[1,2], Gavin L. Foster[1], James W. B. Rae[3], Katy C. Prentice[4], Jonathan Erez[5], Helen C. Bostock[6], Brittney J. Marshall[7], and Paul A. Wilson[1]

[1]Department of Ocean and Earth Science, National Oceanography Centre Southampton, University of Southampton Waterfront Campus, Southampton, UK, [2]Department of Geology and Geophysics, Yale University, New Haven, Connecticut, USA, [3]Department of Earth Sciences, University of St. Andrews, St. Andrews, Scotland, UK, [4]Department of Earth Sciences and Engineering, Imperial College London, London, UK, [5]Institute of Earth Sciences, Hebrew University, Jerusalem, Israel, [6]National Institute for Water and Atmospheric Research, Wellington, New Zealand, [7]Department of Earth and Ocean Sciences, University of South Carolina, Columbia, South Carolina, USA

Abstract B/Ca ratios in foraminifera have attracted considerable scientific attention as a proxy for past ocean carbonate system. However, the carbonate system controls on B/Ca ratios are not straightforward, with $\Delta[CO_3^{2-}]$ ($[CO_3^{2-}]_{in\ situ} - [CO_3^{2-}]_{at\ saturation}$) correlating best with B/Ca ratios in benthic foraminifera, rather than pH, $\frac{B(OH)_4^-}{HCO_3^-}$, or $\frac{B(OH)_4^-}{DIC}$ (as a simple model of boron speciation in seawater and incorporation into $CaCO_3$ would predict). Furthermore, culture experiments have shown that in planktic foraminifera properties such as salinity and $[B]_{sw}$ can have profound effects on B/Ca ratios beyond those predicted by simple partition coefficients. Here, we investigate the controls on B/Ca ratios in *G. ruber* via a combination of culture experiments and core-top measurements, and add to a growing body of evidence that suggests B/Ca ratios in symbiont-bearing foraminiferal carbonate are not a straightforward proxy for past seawater carbonate system conditions. We find that while B/Ca ratios in culture experiments covary with pH, in open ocean sediments this relationship is not seen. In fact, our B/Ca data correlate best with $[PO_4^{3-}]$ (a previously undocumented association) and in most regions, salinity. These findings might suggest a precipitation rate or crystallographic control on boron incorporation into foraminiferal calcite. Regardless, our results underscore the need for caution when attempting to interpret B/Ca records in terms of the ocean carbonate system, at the very least in the case of mixed-layer planktic foraminifera.

1. Introduction

Understanding carbon cycling in the past is key to elucidating the processes that control the Earth's climate system, and ultimately enabling better prediction of the likely effects of future anthropogenic climate change. Given this importance, there is an impetus to develop and hone proxies for the ocean carbonate system. The B/Ca proxy has generated much interest as a potential proxy for the ocean carbonate system, and has already been used to reconstruct past atmospheric CO_2 levels [*Yu et al.*, 2007; *Foster*, 2008; *Tripati et al.*, 2009; *Yu et al.*, 2013]. One reason for such interest is the proposed foundation of the B/Ca proxy in inorganic aqueous chemistry. Boron in seawater is predominantly in one of two forms: the tetrahedrally coordinated borate molecule, $B(OH)_4^-$, and the trigonally coordinated boric acid, or $B(OH)_3$. The relative proportions of the two species are dependent on pH, such that at low pH boron is entirely found in the form of $B(OH)_3$, and at high pH it is found as $B(OH)_4^-$ (see Figure 1). Because $B(OH)_4^-$, the charged ion, is thought to be the only species of boron incorporated into $CaCO_3$, B/Ca ratios in $CaCO_3$ are proposed to increase with a pH-induced increase in the relative abundance of $B(OH)_4^-$ [*Hemming and Hanson*, 1992]. However, recent work has highlighted that a simple two-species model for speciation of boron in seawater may not always be adequate [*Nir et al.*, 2015]. Moreover, the speciation of boron in seawater is not the only control on B/Ca in $CaCO_3$: the site at which boron substitutes into the crystal lattice is also important [e.g., *Paquette and Reeder*, 1995].

The similarity of B–O and C–O bond lengths (0.137 and 0.128 nm, respectively; *Kakihana et al.* [1977]), implies that boron should substitute at the CO_3^{2-} site in $CaCO_3$ as described by Equation (1) below [*Hemming and Hanson*, 1992].

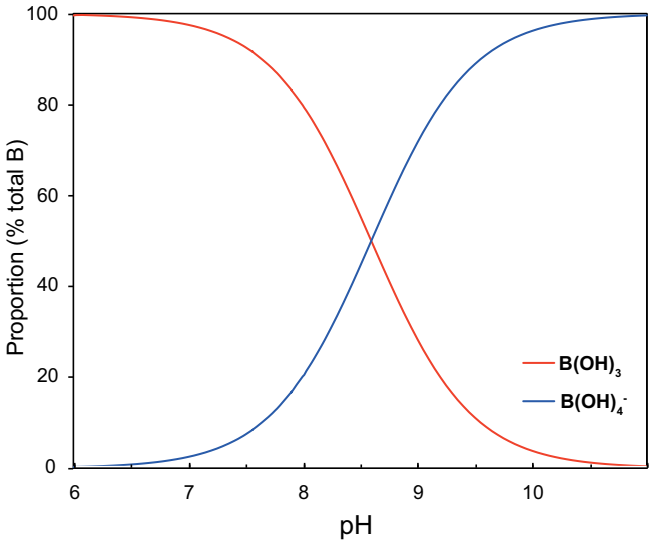

Figure 1. The relative abundances of the two most abundant boron species in seawater, at 25°C and $S = 35$, following *Dickson* [1990]. Boric acid, $B(OH)_3$, is marked in red, while borate ion, $B(OH)_4^-$, is marked in blue.

$$CaCO_{3_{solid}} + B(OH)_{4_{aqueous}}^- \Rightarrow Ca(HBO_3)_{solid} + HCO_{3_{aqueous}}^- + H_2O \quad (1)$$

By extension, the exchange distribution coefficient (K_D) for this reaction was defined as

$$K_D^B = \frac{\left[HBO_3^{2-}/CO_3^{2-}\right]_{solid}}{\left[B(OH)_4^-/HCO_3^-\right]_{fluid}} \quad (2)$$

and later simplified (as in *Yu et al.* [2007]; *Zeebe and Wolf-Gladrow* [2001]) to

$$K_D^B = \frac{[B/Ca]_{solid}}{\left[B(OH)_4^-/HCO_3^-\right]_{fluid}}. \quad (3)$$

More recently, however, culturing work has suggested that the ratio of $B(OH)_4^-$ to total dissolved inorganic carbon may better predict B/Ca ratios when compared to a simple HCO_3^--only model of substitution [*Allen et al.*, 2011, 2012]. In any case, if this mechanism for incorporation is correct, B/Ca ratios in foraminifera should be dependent not only on the pH-driven speciation of boron, but also the speciation of other aqueous compounds (e.g., dissolved inorganic carbon, DIC, compounds CO_3^{2-} and HCO_3^-) that compete for incorporation sites in the carbonate lattice. Furthermore, both boron and DIC speciation is controlled not only by pH, but also by temperature, pressure, and salinity, so each of these variables should have a (more minor) influence on B/Ca in carbonates through their influence on the dissociation constants of DIC (K^*_1, K^*_2) and boric acid (K^*_B) [*Zeebe and Wolf-Gladrow*, 2001].

While inorganic precipitation experiments [*Hemming et al.*, 1995; *Sanyal et al.*, 2000; *He et al.*, 2013] and culture experiments with marine calcifiers [*Sanyal et al.*, 1996, 2001; *Allen et al.*, 2011, 2012, and this study] have demonstrated that pH is indeed a strong control on B/Ca ratios in $CaCO_3$, recent culture experiments [*Allen et al.*, 2011, 2012] show that other factors also influence boron incorporation in foraminiferal calcite. Recent inorganic precipitation experiments have also demonstrated precipitation rate effects on B/Ca ratios [*Gabitov et al.*, 2014; *Uchikawa et al.*, 2015]. Finally, in published open-ocean records, there is already considerable evidence to suggest that the carbonate system is not the only control on recorded B/Ca ratios: for example, (i) a lack of positive correlation between B/Ca ratios and (pH-dependent) boron isotope composition [e.g., *Foster*, 2008, *Palmer et al.*, 2010], (ii) a counterintuitive increase in B/Ca in low-pH upwelling waters relative to nonupwelling conditions [*Naik and Naidu*, 2014], (iii) a lack of correlation between B/Ca and carbonate system conditions in a sediment trap time series [*Babila et al.*, 2014], and (iv) large interspecific differences in B/Ca in planktic foraminifera [e.g., *Yu et al.*, 2007, 2013; *Allen et al.*, 2012], benthic foraminifera [e.g., *Yu and Elderfield*, 2007; *Rae et al.*, 2011], and between planktic and benthic foraminifera [e.g., *Foster*, 2008] that suggest boron incorporation must be, to some extent, biologically mediated. This final point (iv) is in itself perhaps unsurprising given our present understanding of biomineralization processes [e.g., *Erez*, 2003; *Nehrke et al.*, 2013; *de Nooijer et al.*, 2014], although we note that these models of biomineralization are as yet largely inconsistent with boron isotope observations in low Mg-calcite foraminfera [e.g., *Rae et al.*, 2011].

Clearly, then, if we are to make robust paleoceanographic inferences from B/Ca records, we must improve our understanding of the controls on boron incorporation in foraminiferal calcite. Furthermore, as with δ^{11}B-based reconstructions, if B/Ca ratios are to be used to reconstruct past atmospheric pCO_2, it is most crucial to understand boron incorporation in mixed-layer species of foraminifera whose habitat is in communication with the atmosphere. *Globigerinoides ruber* is one such clade: a symbiont-bearing tropical group that consistently records the shallowest stable isotope signatures among the planktic foraminifera [*Hemleben et al.*, 1989]. Here, we examine environmental controls (specifically $\frac{B(OH)_4^-}{DIC}$, temperature, salinity, $[PO_4^{3-}]$,

and bottom water $\Omega_{calcite}$) on boron concentration in shells of this mixed-layer foraminifera from core-tops, sediment traps, and cultures, and thereby test the utility of B/Ca in this species as a tool for ocean carbonate system reconstruction. Also, because this clade is now thought to be a grouping of several genetically and morphologically distinct species [e.g., *Aurahs et al*., 2011], and because there is some suggestion that B/Ca ratios might change with test size [*Ni et al*., 2007], we investigate whether boron incorporation patterns differ between *G. ruber* sensu stricto and sensu lato [*Wang*, 2000] and across commonly-used size fractions.

2. Methods

2.1. Culture Experiments on *G. ruber*

Data from cultured *G. ruber* comes from the experiments of *Henehan et al*. [2013] (details of culturing protocol and carbonate system control reported therein). In brief, mixed morphotypes of *G. ruber* (sensu stricto and sensu lato; *Wang*, [2000]) were cultured at a constant temperature (26 ± 0.5 °C), salinity (37.2) and light levels (13 h light:11 h dark), but at three different pH treatments (8.174 ± 0.007, 7.894 ± 0.013, and 7.554 ± 0.013; total scale ± 2 s.e.). Me/Ca ratios for cultured material are obtained via mass-balance calculations to remove mass grown out of culture, as described in equation (4) below.

$$Me/Ca_{culture} = \frac{Me/Ca_{bulk} - (\frac{Me}{Ca}_{controls} \times P^{mass}_{controls})}{P^{mass}_{culture}} \quad (4)$$

$P^{mass}_{controls}$ is the proportion of mass calcified prior to culture, while $P^{mass}_{culture}$ is the proportion of mass grown in culture. To determine $P^{mass}_{controls}$, initial preculture mass was determined from starting dimensions using the calculated size-to-mass relationship from *Henehan et al*. [2013], and end-culture mass was determined by weighing cultured tests. $Me/Ca_{controls}$ is the trace element composition of *G. ruber* towed at the time of the collection of cultured individuals, while Me/Ca_{bulk} is the measured trace element ratio in post culture material.

2.2. Site and Sample Selection

To investigate the controls on B/Ca ratios in foraminifera grown outside of culture conditions, *G. ruber* were analyzed from geographically disparate core-top sites (from archives at Tübingen and NIWA, Wellington). These samples were verified as late Holocene (<3 ka) via C14 dating or presence of living benthic foraminifera. In addition, sediment trap sample material from the Cariaco Basin and towed specimens from the Gulf of Aqaba (Eilat) were analyzed, with the aim of investigating post depositional alteration. Core-top B/Ca data from *Foster* [2008] are also included in statistical analyses, but with carbonate system parameters reestimated following *Henehan et al*. [2013] for consistency. The locations of these sample sites are shown in Figure 2. Morphotypes of *G. ruber* were separated for B/Ca analysis according to the definition of *Wang* [2000]: sensu stricto (Type I) and sensu lato (encompassing "platy" type IIa and "elongate" type IIb; *Numberger et al*. [2009], *Aurahs et al*. [2011]), although in some cases (Sites MC394, GGC48, GeoB1208-2, and Gulf of Aqaba tows) sample size limitations meant morphotypes were combined.

2.3. Characterization of Carbonate System and Hydrographic Properties

Carbonate system calculations for culture experiments and open ocean sites are described in *Henehan et al*. [2013]. In brief, culture conditions are the mean carbonate system, temperature, and salinity conditions experienced by each foraminifera, weighted to the mass each individual contributed to the bulk measurement. Nutrient data for these experiments are based on measurements of preculture and post culture seawater. For core-top samples, preindustrial carbonate system estimates are derived from the *Takahashi et al*. [2009] database of global SST, salinity and CO_2 fluxes, and modeled estimates of postindustrial changes in CO_2 flux from *Gloor et al*. [2003]. Mean annual surface water [PO_4^{3-}] at each site is obtained from World Ocean Atlas (WOA) [*Garcia et al*., 2010], and deep-water $\Omega_{Calcite}$ is taken from nearby GLODAP and CARINA sites [*Key et al*., 2004, 2010]. Through this broad sampling of core-top locations, B/Ca could be measured in foraminifera across a large range in pH (8.06–8.21), temperature (14–30°C), salinity (34.61–40.7), carbonate saturation state at site of deposition (0.98–5.52) and nutrient concentration ([PO_4^3] = 0.06–0.48 μmol/kg).

Although calculations of preindustrial pH used here are derived from the *Takahashi et al*. [2009] surface water database, MOCNESS tows by *Kuroyanagi and Kawahata* [2004] found that *G. ruber* sensu lato were abundant at depths of >50 m (as opposed to peak abundance of *G. ruber* sensu stricto at <20 m depth).

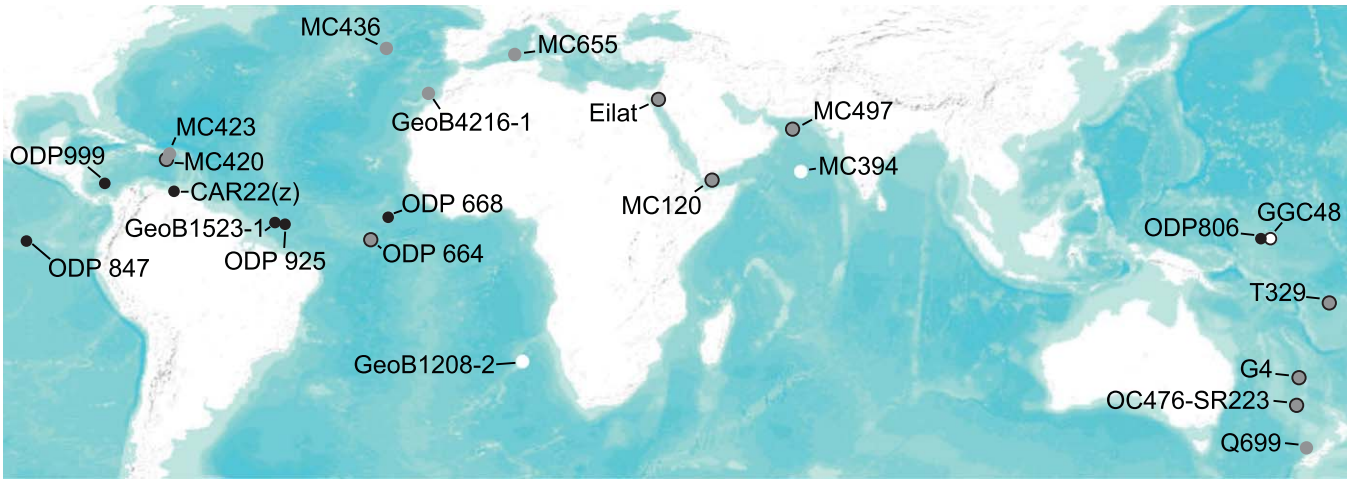

Figure 2. Locations of core-top and sediment trap samples used in this study. White circles are mixed morphotype coretop sites, gray circles are *G. ruber* sensu lato only, black circles are *G. ruber* sensu stricto only, white circles with a black outline are sites where mixed morphotype and *G. ruber* sensu stricto only measurements were taken, and gray circles with a black outline are sites where both morphotypes were measured.

This deeper habit in *G. ruber* sensu lato is corroborated by $\delta^{18}O$ and Mg/Ca-derived calcification temperatures [*Wang*, 2000; *Löwemark et al*., 2005; *Kawahata*, 2005; *Steinke et al*., 2005, 2008]. We therefore also estimated preindustrial hydrographic parameters at a depth of 50 m by applying local modern surface-to-50 m pH, temperature and salinity gradients from GLODAP [*Key et al*., 2004] and CARINA [*Key et al*., 2010] datasets to our reconstructed preindustrial surface values.

Collinearity of oceanic variables is often a problem in differentiating competing influences on proxy signals (see discussions in *Allen et al*. [2012], *Marshall et al*. [2013]), and as such we test for this in the sample set used in multivariate analyses (see Figure 3). Significant correlations exist between temperature and carbonate system parameters (pH and $\frac{B(OH)_4^-}{DIC}$; $R^2 = 0.17$ and 0.28, respectively), and between salinity and $\frac{B(OH)_4^-}{DIC}$.

2.4. Sample Preparation

Foram cleaning was largely as described in *Rae et al*. [2011] and *Henehan et al*. [2013], which in turn is based on the approach of *Barker et al*. [2003]. Foraminiferal samples of 1–3 mg (to permit boron isotope analysis on the same samples where possible; see *Henehan et al*. [2013]) were lightly crushed between two clean glass slides, ultrasonicated and rinsed repeatedly with Milli-Q ultrapure water (18.2 MΩ) to remove clays. For tow and sediment trap samples (where clay is not a major contaminant), as few as three rinses were carried out (to minimize sample loss), but in core-top samples five or more rinses were required to ensure efficient removal of clay material. Culture, sediment trap and tow samples, in agreement with other culturing studies [e.g., *Russell et al*., 2004], were subject to intensified oxidative cleaning (3 × 20–30 min treatments of 250–400 μL (depending on sample size) 1% H_2O_2 in 0.1 *M* NH_4OH at 80°C) to account for the larger organic content. In core-tops, oxidative cleaning was shorter (3 × 5 min) to minimize sample loss. Samples were then subject to a brief weak acid leach in 0.0005 *M* HNO_3 to remove any readsorbed contaminants. Finally 200 μL of Milli-Q was added to each sample (to slow subsequent dissolution and reduce the likelihood of leaching of B off any remnant contaminants) and 0.5 *M* HNO_3 (normally $<$ 300 μL) added incrementally until the sample was fully dissolved. To ensure complete removal of clays and other contaminants, samples were centrifuged for $>$5 min at 1400 rpm, and the supernatant removed to a clean vial, leaving the last $\sim$20 μL to be discarded.

2.5. ICP-MS Analysis

Trace element analysis was carried using a Thermo Element ICP-MS at the University of Southampton (UoS; core-tops and sediment traps) and the Bristol Isotope Group (BIG; cultures and tows). Analysis of common consistency standards ensures no bias exists between these two laboratories in measurement of trace elements ratios (e.g., B/Ca, Li/Ca, Mg/Ca, Sr/Ca etc). This is despite slight differences in sample introduction systems: typical Ar sample gas flow through the nebulizer at BIG is $\sim$1.2 L/min, while at UoS sample gas input

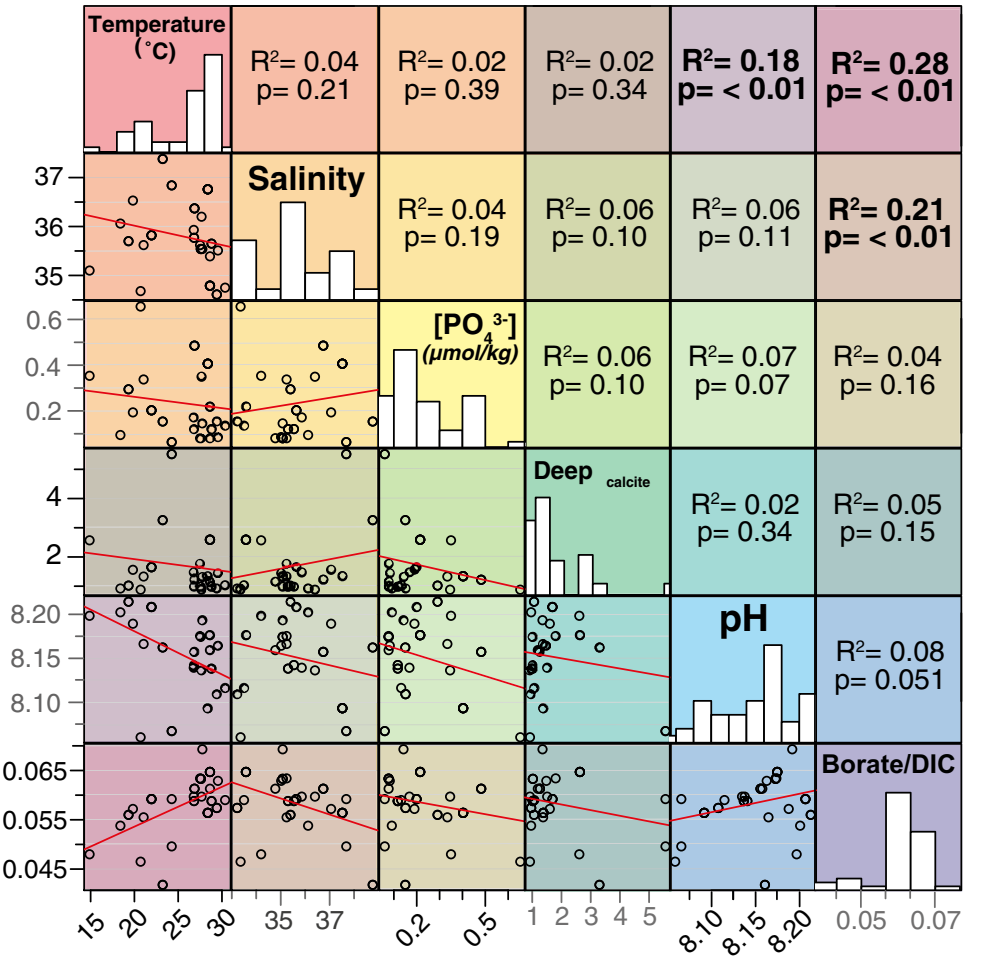

Figure 3. A matrix of crossplots and R^2 values of linear regressions between the environmental parameters used in multiple regression models. Font size in R^2 values scales with the strength of the relationship. Histograms for each variable describe frequency distributions in each case.

is fixed at 0.7 L/min, and an additional Ar gas supply (typically to ~0.4–0.45 L/min) is added directly into the spray chamber. In both laboratories Teflon barrel spray chambers are used, and NH_3 (7 mL/min) is added to aid washout (following *Al-Ammar et al.* [2000]).

Tuning is performed on a 0.1 ppb multielement tune solution (with 0.5 ppb of Boron) to optimize sensitivity while minimizing the presence of oxides (UO is monitored and UO:U counts are kept to <7 %). Typical counts for B, In and U are 40–100 kcps/ppb, 700–1000 kcps/ppb, and 1000–1400 kcps/ppb, respectively (at an uptake rate of ~80 µL/min). During each analytical session, in-house consistency standards (B/Ca ratios of ~197, 496, and 32 µmol/mol, respectively) were analyzed at a range of concentrations (typically 0.5, 1, and 2 m*M* Ca) to monitor machine performance. Reproducibility of element ratio measurements is optimized [*Yu et al.*, 2005] by matrix-matching samples and their bracketing standards (in this study in-house gravimetric standard). This is achieved by analyzing for [Ca] in a diluted aliquot of each sample (typically 20 µL in 200 µL 0.5 *M* HNO_3) prior to full elemental determination. Samples are then diluted with 0.5 *M* HNO_3 to match standard [Ca] and analyzed for the full trace metal suite. Long-term reproducibility of B/Ca ratio measurements is better than 5% (2 sd), based on repeat measurements of in-house consistency standards.

2.6. Statistical Analyses

To determine which if any of the factors parameterized here (temperature, salinity, $[PO_4^{3-}]$, bottom water $\Omega_{calcite}$, test size, morphotype and $\frac{B(OH)_4^-}{DIC}$) have significant effects on foraminiferal B/Ca, multiple linear regression analyses were carried out (on both the whole data set and on separate morphospecies-specific groupings) using R statistical software (http://www.r-project.org). Noncontributing parameters were

Table 1. Results of Culture Experiments in *G. ruber*[a]

Experiment	Temperature (°C)	±	Salinity (psu)	±	pH (total)	±	$[CO_3^{2-}]$ (μmol/kg)	$\Delta[CO_3^{2-}]$ (μmol/kg)	$[B(OH)_4^-]$ HCO_3^-	$[B(OH)_4^-]$ DIC	B/Ca (μmol/mol)	±
Higher pH	26	0.5	37.2	0	8.183	0.007	296.9	296.9	0.0804	0.0679	190.2	13.4
Midrange pH	26	0.5	37.2	0	7.895	0.013	164.2	164.2	0.0449	0.0408	155.8	11.0
Low pH	26	0.5	37.2	0	7.566	0.013	79.4	79.4	0.0225	0.0212	125.5	8.9

[a]pH is calculated as the mean of the average pH observed by each individual foraminifera during culture (as measured using a potentiometric electrode but cross-calibrated to DIC/TAlk-derived pH via a correction factor of −0.21, see *Henehan et al*. [2013]). Uncertainty on culture pH measurements is 2 standard errors of the mean of the average pHs experienced by constituent foraminifera. $\frac{B(OH)_4^-}{HCO_3^-}$ or $\frac{B(OH)_4^-}{DIC}$ estimates are derived from pH and alkalinity measurements using CO2sys [*van Heuven et al*., 2011]. Uncertainty on culture B/Ca is estimated as a quadratic addition of 5% errors in culture and control measurements.

removed from models according to their contribution to the model's Akaike Information Criterion (AIC) [*Akaike*, 1974]. This parameter describes the relative quality of each of a set of statistical models derived from a set of data, based on the compromise between the complexity of each model and its goodness-of-fit. Thus, if the addition of a parameter makes no positive contribution to the AIC, the parameter is omitted from the model. After this stepwise removal of noncontributing factors, the relative importance (i.e., relative contribution to the overall model R^2) of each remaining parameter is further illustrated using the *relaimpo* package [*Groemping*, 2006] for *R*. Following the recommendation of *Groemping* [2006], we estimate these relative importance via the "lmg" approach, based on the work of *Lindeman et al*. [1980]. This removes an otherwise sizeable influence of factor ordering (i.e., which factor is entered into the model first) on the relative importance metric, by averaging out relative importance computed from all factor ordering permutations. 95% confidence intervals on these relative importance are calculated via bootstrapping, with 1000 repeated samplings from the residuals of the regression model (following *Hesterberg et al*. [2005]).

3. Results

3.1. B/Ca in Cultured *G. ruber*

B/Ca ratios from cultured *G. ruber* (white) range from 120 to 180 μmol/mol and show a strong positive correlation with pH, $\frac{B(OH)_4^-}{HCO_3^-}$ and $\frac{B(OH)_4^-}{DIC}$ (Table 1 and Figure 4). Compared to cultures of *G. ruber* (pink) [*Allen et al*., 2012], these new data show much more linear relationships between B/Ca and these carbonate system parameters.

3.2. B/Ca in *G. ruber* from Tows, Core-Tops and Sediment Traps

B/Ca measurements in tow, core-top and sediment trap samples of *G. ruber* are given in Table 2. Despite exhibiting a relatively small range in *in situ* pH, $\frac{B(OH)_4^-}{HCO_3^-}$ or $\frac{B(OH)_4^-}{DIC}$ compared to that seen in cultured samples, B/Ca values span an even greater range (∼90–180 μmol/mol) than those seen in culture (120–200 μmol/mol; see Figure 5). Also, unlike in benthic foraminifera [*Yu and Elderfield*, 2007; *Rae et al*., 2011; *Brown et al*., 2011; *Raitzsch et al*. 2011; *Yu et al*. 2013], there is no correlation evident between B/Ca and $\Delta[CO_3^{2-}]$ ($R^2 = 0.03$; see supporting information Figure S1). Regression plots against other environmental parameters ($[PO_4^{3-}]$, salinity, $\Omega_{Calcite}$ at the site of deposition, and sea surface temperature), morphotype and test size are shown in red in Figure 6. To better determine the nature of other controlling factors on boron incorporation, the effect of $\frac{B(OH)_4^-}{DIC}$ seen in culture (the strongest controlling factor in cultures from *Allen et al*. [2012] and this study, Figure 4) was removed, and the residual variation from the linear B/Ca-$\frac{B(OH)_4^-}{DIC}$ culture relationship ($B/Ca = 1378.2(\frac{B(OH)_4^-}{DIC}) + 97.51$; see Figure 4) was examined. Correlations between environmental parameters and residual variation from the culture B/Ca-$\frac{B(OH)_4^-}{DIC}$ relationship are shown in blue (Figure 6).

No clear correlations are seen in raw or residual B/Ca with deep-water calcite saturation state, temperature, or size. In both raw and residual B/Ca, the strongest correlations are instead seen with salinity and surface water $[PO_4^{3-}]$ (Figure 6). Although salinity is somewhat negatively correlated with $\frac{B(OH)_4^-}{DIC}$ ($R^2 = 0.21$; Figure 3), because correlation of B/Ca with $\frac{B(OH)_4^-}{DIC}$ is poor (Figure 5), and because comparing residual variation from the culture-derived B/Ca-$\frac{B(OH)_4^-}{DIC}$ relationship in Figure 4 strengthens the effect of salinity (see Figure 6), we conclude that the observed effect of salinity on B/Ca is not derived from collinearity with $\frac{B(OH)_4^-}{DIC}$. $[PO_4^{3-}]$ is not significantly correlated with other carbonate system or hydrographic variables (Figure 3), and its influence on B/Ca also appears robust. Further evidence of the influence of $[PO_4^{3-}]$ is seen in three tow samples

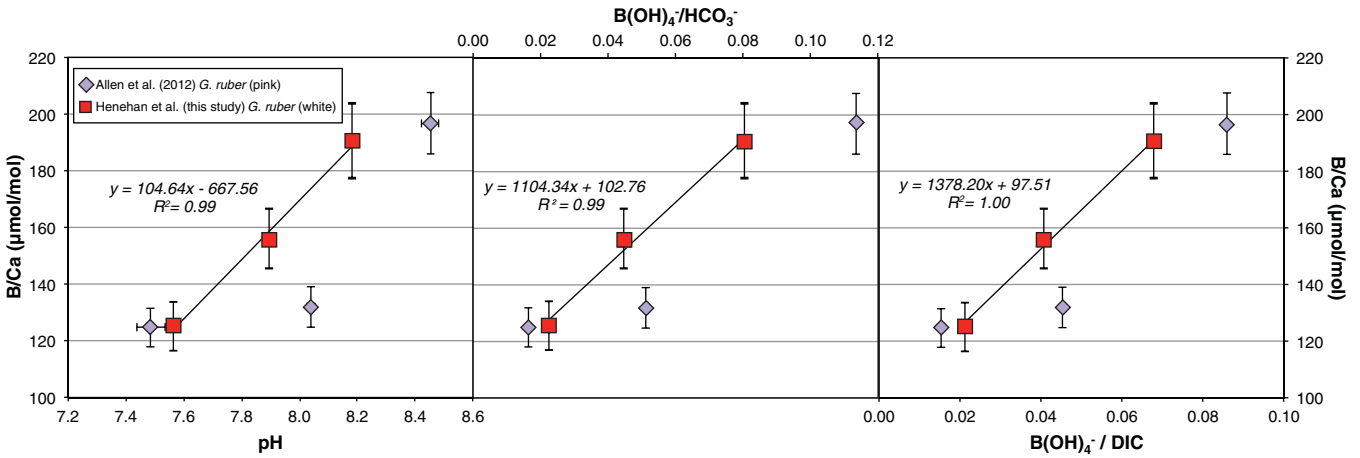

Figure 4. Changes in B/Ca ratios observed in cultures of *G. ruber*, in response to carbonate system changes. Also plotted are data from *G. ruber* (pink) from *Allen et al*. [2012]. Error bars for B/Ca ratios in *G. ruber* (white) are 5% analytical uncertainty, while for *G. ruber* (pink) they are as stated in *Allen et al*. [2012].

from the Gulf of Aqaba (Eilat) sampled between January and March 2010, whose B/Ca are very strongly correlated to $[PO_4^{3-}]$, (with a slope almost identical to that seen in core-tops) but not to pH (see Table 2 and Figure 7).

3.3. Multiple Regression Models

The interference of multiple variables on B/Ca incorporation results in low correlation coefficients for single-variable-B/Ca regressions fits (as seen in Figure 6). Multiple regression analyses are therefore useful in disentangling the determinant factors. Results of multiple regression analyses of both the entire data set and morphotype-specific groupings are given in Table 3 and supporting information Tables S1–S3. No model finds $\frac{B(OH)_4^-}{DIC}$ to be a major control on B/Ca ratios; instead most variance is explained by changes in $[PO_4^{3-}]$ and salinity. The relative importance of each factor, calculated using "relaimpo" [*Groemping*, 2006] is illustrated in Figure 8. Although we combine data from multiple size fractions at some sites in our models (to improve statistical power), using 300–355 µm size fraction only also finds $[PO_4^{3-}]$ and salinity to be the most influential factors, suggesting there is no major effect of pseudo-replication.

It should be noted, however, that high-salinity core-top and tow samples from Gulf of Aqaba (Eilat) (both sensu stricto and sensu lato, as shown in red in Figure 5 and in grey in Figure 6) were found to be significant outliers that bias multiple regression models, as signified by Cook's distances of >1 [*Cook and Weisberg*, 1982]. Specifically, Gulf of Aqaba (Eilat) salinity is anomalously high ($\geq$40.4), but B/Ca measurements are not as high as salinity trends in the rest of the data would suggest (Figure 6b). Although models including core-top and tow data from Eilat still detect a significant effect of $[PO_4^{3-}]$ and salinity, their inclusion of renders meaningful analysis of other data difficult, so we omit these data points from multivariate statistical analyses. The significance of this omission is discussed in section 4.8.

The influence of test size on B/Ca is small but statistically discernible (Table 3). Multiple regression models of *G. ruber* sensu stricto alone, however (supporting information Table S1 and Figure 8), detect no effect of size on B/Ca; the signal derives only from measurements of *G. ruber* sensu lato (Figure 8; see also supporting information Table S2). This differential change in B/Ca with size across morphotypes is illustrated further in Figure 9. In analysis of *G. ruber* B/Ca (all morphotypes; Table 3), though, morphotype is discounted from the model as a nonsignificant factor, on the basis of deterioration in AIC score. Moreover, there is no significant difference in B/Ca (paired two-tail *t*-test, $p = 0.520$, $n = 10$) between the two morphotypes at sites where both *G. ruber* sensu stricto and sensu lato of the same size were measured. Despite this, multivariate regression analysis of the sensu stricto morphotype alone results in better model fits ($R^2_{(adjusted)} = 0.72$; supporting information Table S1) than analyses of either the whole data set ($R^2_{(adj.)} = 0.60$; Table 3) or sensu lato data only ($R^2_{(adj.)} = 0.54$; supporting information Table S2). This difference in goodness-of-fit is, however, less pronounced when a habitat depth of 50 m is assumed for *G. ruber* sensu lato ($R^2_{(adj.)} = 0.65$, supporting information Table S3).

Table 2. Summary of Core-Top, Tow (Gulf of Aqaba, Eilat) and Sediment Trap (CAR 22(z) only) Samples of *G. ruber* Analyzed Here

Site	Description	Size Fraction (μm)	Lat (°N)	Long (°E)	Temperature (°C)	± (°C)	Salinity	±	Deep $\Omega_{calcite}$	$[PO_4^{3-}]$ (μmol/kg)	Total Alkalinity (μmol/kg)	DIC (μmol/kg)	pH (total)	±	Borate/ Bicarbonate	Borate/ DIC	B/Ca (μmol/mol)	Residual B/Ca (μmol/mol)
MC394	Mixed morph	300–355	14.38	64.57	27.67	2.24	36.20	0.35	0.88	0.346	2365.5	1969.4	8.135	0.020	0.0699	0.0597	136.3	−43.6
GGC48	Mixed morph	250–300	0.00	161.00	29.41	0.36	34.61	0.51	0.92	0.151	2276.1	1905.3	8.108	0.064	0.0668	0.0574	95.6	−81.1
GeoB1208-2[a]	Mixed morph	300–355	−24.49	7.11	21.05	3.64	35.62	0.19	1.33	0.334	2341.0	1991.4	8.165	0.044	0.0635	0.0555	112.0	−62.0
Eilat tow (27 Jan 2010)	Mixed morph	279	29.50	34.92	22	0.5	40.4	0.10	n/a	0.3	2500.4	2110.4	8.128	0.005	0.0681	0.0592	110.29	−68.8
Eilat tow (8 Feb 2010)	Mixed morph	209	29.50	34.92	23	0.5	40.32	0.10	n/a	0.14	2507.7	2114.6	8.116	0.005	0.0679	0.0589	99.39	−79.3
Eilat tow (7 Mar 2010)	Mixed morph	279	29.50	34.92	23	0.5	40.44	0.10	n/a	0.41	2500.3	2116.1	8.103	0.005	0.0663	0.0578	120.90	−56.2
MC655	*sensu lato*	250–300	38.42	5.40	23.23	3.00	37.38	0.20	3.26	0.15	2580.0	2225.0	8.161	0.050	0.0460	0.0418	116.6	−38.5
T329	*sensu lato*	250–300	−12.96	173.57	28.63	1.45	34.79	0.24	2.59	0.215	2287.7	1876.2	8.175	0.023	0.0766	0.0647	89.2	−97.4
MC120	*sensu lato*	250–300	12.47	45.38	28.38	5.55	36.76	1.23	1.34	0.403	2396.7	2013.6	8.092	0.068	0.0656	0.0564	136.4	−38.8
Eilat	*sensu lato*	250–300	29.50	34.92	23.76	4.25	40.40	0.22	4.48	0.129	2509.5	2058.4	8.192	0.008	0.0803	0.0679	119.4	−71.8
Q699	*sensu lato*	250–355	−42.42	169.30	14.88	3.53	35.10	0.25	2.57	0.35	2315.7	2018.5	8.197	0.005	0.0538	0.0480	127.9	−35.7
MC655	*sensu lato*	300–355	38.42	5.40	23.23	3.00	37.38	0.20	3.26	0.15	2580.0	2225.0	8.161	0.050	0.0460	0.0418	141.5	−13.5
MC120	*sensu lato*	300–355	12.47	45.38	28.38	5.55	36.76	1.23	1.34	0.403	2396.7	2013.6	8.092	0.068	0.0656	0.0564	145.5	−29.8
ODP 664	*sensu lato*	300–355	0.10	−23.23	26.81	3.97	35.77	0.35	0.98	0.117	2341.3	1956.8	8.141	0.008	0.0685	0.0588	119.4	−59.1
G4	*sensu lato*	300–355	−28.42	167.25	21.95	3.98	35.82	0.11	1.65	0.199	2360.7	1978.9	8.207	0.030	0.0686	0.0592	122.2	−56.8
MC436	*sensu lato*	300–355	39.80	−21.06	18.40	3.74	36.06	0.09	0.92	0.091	2365.2	2021.0	8.201	0.018	0.0614	0.0538	116.0	−55.7
MC497	*sensu lato*	300–355	23.53	63.31	26.86	3.64	36.37	0.21	1.22	0.482	2375.7	1970.2	8.156	0.020	0.0719	0.0613	165.1	−16.9
MC423	*sensu lato*	300–355	17.75	−65.59	27.50	2.00	35.62	0.82	1.76	0.077	2342.2	1929.1	8.174	0.012	0.0748	0.0634	133.5	−51.4
T329	*sensu lato*	300–355	−12.96	173.57	28.63	1.45	34.79	0.24	2.59	0.215	2287.7	1876.2	8.175	0.023	0.0766	0.0647	113.9	−72.7
GeoB4216-1[a]	*sensu lato*	300–355	30.63	−12.40	19.83	3.84	36.53	0.13	1.56	0.19	2394.2	2028.4	8.188	0.006	0.0657	0.0572	121.6	−54.8
OC476-SR223	*sensu lato*	300–355	−33.53	166.53	19.33	3.74	35.70	0.13	1.02	0.291	2352.7	1995.1	8.213	0.014	0.0643	0.0560	102.5	−72.3
MC420	*sensu lato*	355–400	17.04	−66.00	27.59	1.08	35.54	0.48	0.98	0.077	2337.9	1926.0	8.173	0.013	0.0747	0.0633	110.8	−74.0
G4	*sensu lato*	355–400	−28.42	167.25	21.95	3.98	35.82	0.11	1.65	0.199	2360.7	1978.9	8.207	0.030	0.0686	0.0592	136.4	−42.6
MC120	*sensu stricto*	250–300	12.47	45.38	28.38	5.55	36.76	1.23	1.34	0.403	2396.7	2013.6	8.092	0.068	0.0656	0.0564	132.9	−42.4
CAR22(z)	*sensu stricto*	250–300	10.50	−64.66	24.26	1.97	36.84	0.11	5.52	0.06	2411.6	2081.8	8.066	0.018	0.0562	0.0592	121.5	−57.6
T329	*sensu stricto*	250–300	−12.96	173.57	28.63	1.45	34.79	0.24	2.59	0.215	2287.7	1876.2	8.175	0.023	0.0766	0.0647	141.0	−45.6
GGC48	*sensu stricto*	250–300	0.00	161.00	29.41	0.36	34.61	0.51	0.92	0.151	2276.1	1905.3	8.108	0.064	0.0668	0.0574	99.1	−77.5
Eilat	*sensu stricto*	250–300	29.50	34.92	23.76	4.25	40.40	0.22	4.48	0.129	2509.5	2058.4	8.192	0.008	0.0803	0.0679	121.3	−69.8
OC476-SR223	*sensu stricto*	250–355	−33.53	166.53	19.33	3.74	35.70	0.13	1.02	0.291	2352.7	1995.1	8.213	0.014	0.0643	0.0560	95.1	−79.6
MC120	*sensu stricto*	300–355	12.47	45.38	28.38	5.55	36.76	1.23	1.34	0.403	2396.7	2013.6	8.092	0.068	0.0656	0.0564	144.9	−30.4
MC120	*sensu stricto*	300–355	12.47	45.38	28.38	5.55	36.76	1.23	1.34	0.403	2396.7	2013.6	8.092	0.068	0.0656	0.0564	166.0	−9.3
MC497	*sensu stricto*	300–355	23.53	63.31	26.86	3.64	36.37	0.21	1.22	0.482	2375.7	1970.2	8.156	0.020	0.0719	0.0613	160.6	−21.4
ODP 664	*sensu stricto*	300–355	0.10	−23.23	26.81	3.97	35.77	0.35	0.98	0.117	2341.3	1956.8	8.141	0.008	0.0685	0.0588	107.4	−71.1
G4	*sensu stricto*	300–355	−28.42	167.25	21.95	3.98	35.82	0.11	1.65	0.199	2360.7	1978.9	8.207	0.030	0.0686	0.0592	119.7	−59.4
CAR22(z)	*sensu stricto*	300–355	10.50	−64.66	24.26	1.97	36.84	0.11	5.52	0.06	2411.6	2081.8	8.066	0.018	0.0562	0.0496	129.7	−36.2
GGC48	*sensu stricto*	300–355	0.00	161.00	29.41	0.36	34.61	0.51	0.92	0.151	2276.1	1905.3	8.108	0.064	0.0668	0.0574	103.2	−73.5
T329	*sensu stricto*	300–355	−12.96	173.57	28.63	1.45	34.79	0.24	2.59	0.215	2287.7	1876.2	8.175	0.023	0.0766	0.0647	131.1	−55.6
T329	*sensu stricto*	300–355	−12.96	173.57	28.63	1.45	34.79	0.24	2.59	0.215	2287.7	1876.2	8.175	0.023	0.0766	0.0647	144.7	−42.0
MC120	*sensu stricto*	300–355	12.47	45.38	28.38	5.55	36.76	1.23	1.34	0.403	2396.7	2013.6	8.092	0.068	0.0656	0.0564	136.7	−38.6
MC420	*sensu stricto*	300–355	17.04	−66.00	27.59	1.08	35.54	0.48	0.98	0.077	2337.9	1926.0	8.173	0.013	0.0747	0.0633	110.9	−73.8
MC420	*sensu stricto*	355–400	17.04	−66.00	27.59	1.08	35.54	0.48	0.98	0.077	2337.9	1926.0	8.173	0.013	0.0747	0.0633	117.8	−66.9
MC497	*sensu stricto*	355–400	23.53	63.31	26.86	3.64	36.37	0.21	1.22	0.482	2375.7	1970.2	8.156	0.020	0.0719	0.0613	178.4	−3.6
G4	*sensu stricto*	355–400	−28.42	167.25	21.95	3.98	35.82	0.11	1.65	0.199	2360.7	1978.9	8.207	0.030	0.0686	0.0592	114.1	−65.0
T329	*sensu stricto*	355–400	−12.96	173.57	28.63	1.45	34.79	0.24	2.59	0.215	2287.7	1876.2	8.175	0.023	0.0766	0.0647	114.7	−71.9
ODP 847[a]	*sensu stricto*	300–355	0.20	−95.32	24.50	1.40	34.20	0.26	0.88	0.653	2257.4	1962.5	8.059	0.056	0.0526	0.0465	115.3	−46.4
ODP 925[a]	*sensu stricto*	300–355	4.20	−43.48	27.73	0.77	35.58	0.81	1.47	0.168	2343.6	1950.2	8.138	0.004	0.0699	0.0597	113.8	−66.0
ODP 664[a]	*sensu stricto*	300–355	0.10	−23.23	26.81	3.97	35.77	0.35	0.98	0.117	2341.3	1956.8	8.137	0.073	0.0685	0.0588	108.0	−70.5
ODP 668[a]	*sensu stricto*	300−355	4.77	−20.93	27.75	0.70	35.40	0.24	1.44	0.082	2313.5	1909.6	8.163	0.018	0.0741	0.0629	112.4	−71.8
ODP 999[a]	*sensu stricto*	300–355	12.75	−78.73	27.88	0.98	35.77	0.32	1.15	0.077	2363.0	1955.6	8.158	0.019	0.0720	0.0613	119.5	−62.5
ODP 806[a]	*sensu stricto*	300–355	0.32	159.37	29.50	0.19	34.53	0.25	1.03	0.132	2270.4	1891.8	8.115	0.023	0.0689	0.0590	111.0	−67.8
GeoB1523-1	*sensu stricto*	300–355	3.83	−41.62	27.72	0.74	35.75	0.62	1.31	0.142	2332.8	1896.2	8.192	0.042	0.0826	0.0693	113.4	−79.6
ODP 664	*sensu stricto*	355–425	0.10	−23.23	26.81	3.97	35.77	0.35	0.98	0.117	2341.3	1956.8	8.141	0.008	0.0685	0.0588	113.7	−64.9

[a]Sites marked are taken from *Foster* [2008]. For these sites, carbonate system parameters were re-estimated via the methods of Henehan et al. [2013] for consistency with the rest of the data set.

Carbonate system parameters are estimated as in *Henehan et al.* [2013]. $[PO_4^{3-}]$ measurements are surface measurements from the nearest World Ocean Atlas data point [*Garcia et al.*, 2010], except in the case of Gulf of Aqaba (Eilat) tow samples, where $[PO_4^{3-}]$ was measured. Size fraction is based on sieve range, except in Gulf of Aqaba (Eilat) tow samples, where average test size was measured. Uncertainty on temperature, salinity, and pH is the two standard deviations of intra-annual variability in these $B(OH)_4^-$ parameters at each site, except in Gulf of Aqaba (Eilat) tow samples, where it is estimated measurement error. Residual B/Ca is the measured B/Ca minus the predicted B/Ca from the culture B/Ca–$\frac{B(OH)_4^-}{DIC}$ relationship, and is used to better test for other controlling factors.

A small but discernible effect of deep-water carbonate saturation state on B/Ca is revealed in regression models of all data and sensu stricto morphotypes only (Table 3 and Figure 8). However, no significant correlation with temperature is detected in any model. It is worth noting, finally, that fitting of multiplicative models (allowing interaction of variables) resulted in poorer fits, and as such these models are not discussed here.

4. Discussion

4.1. Carbonate System Control on B/Ca Ratios

These new data suggest that the marine carbonate system has very little influence on B/Ca in open ocean samples of *G. ruber*. Instead $[PO_4^{3-}]$ and salinity, appear to be the dominant controls. This finding contrasts with evidence from cultures [*Sanyal et al*., 1996; *Allen et al*., 2011, 2012; this study] (Figure 4), and therefore implies interference from competing controls on boron incorporation in the natural environment. Multiple regression in *G. ruber* sensu stricto morphotype detects a small but statistically significant (to 95% confidence) effect of $\frac{B(OH)_4^-}{DIC}$ on B/Ca (supporting information Table S1), but when these data are combined with measurements of *G. ruber* sensu lato this effect disappears (note that inclusion of pH or $\frac{B(OH)_4^-}{HCO_3^-}$ in lieu of $\frac{B(OH)_4^-}{DIC}$ has no bearing on this finding).

While the carbonate system cannot then be considered a strong control on B/Ca in these open ocean samples, in all cases multiple regression models were slightly more powerful (i.e., had a higher $R^2_{(adj.)}$) when the residuals from the culture $\frac{B(OH)_4^-}{DIC}$ –B/Ca relationship were analyzed in lieu of raw B/Ca ratios: sensu stricto $R^2_{(adj.)}$ 0.74 → 0.75, sensu lato $R^2_{(adj.)}$ 0.54 → 0.63, both $R^2_{(adj.)}$ 0.60 → 0.65. Analysis of these residuals rather than B/Ca did not affect which environmental parameters proved to be controls or the relative importance of these factors, except in the case of *G. ruber* sensu lato, where size was no longer found to be a significant factor in multiple regression analysis of residual B/Ca. These marginal improvements in model fit may conceivably hint at a small underlying influence of $\frac{B(OH)_4^-}{DIC}$ on B/Ca that is obscured by conflicting factors. Note that no detectable difference arises from using the residuals from the $\frac{B(OH)_4^-}{DIC}$ –B/Ca relationship from *G. ruber* (pink) [*Allen et al*., 2012] instead of the new culture relationship for *G. ruber* (white) presented here.

4.2. $[PO_4^{3-}]$: A Previously Undocumented Control on B/Ca Ratios

The positive correlation between phosphate concentrations ($[PO_4^{3-}]$) and B/Ca seen in these core-top data is the first documentation of $[PO_4^{3-}]$ influencing boron incorporation in planktic foraminifera, and is independent of any collinearity of $[PO_4^{3-}]$ with other environmental variables (see Figure 3). While this correlation is perhaps initially surprising, it is consistent with the findings of *Naik and Naidu* [2014], who show higher B/Ca in *G. ruber* from upwelling waters (i.e., higher in $[PO_4^{3-}]$), despite their lower pH. Although $[PO_4^{3-}]$ is somewhat correlated in our data set with concentrations of other nutrients such as silicate and nitrate, these variables do not correlate as strongly with core-top foraminiferal B/Ca as $[PO_4^{3-}]$, and are discounted as nonsignificant factors when tested in multiple regression models alongside $[PO_4^{3-}]$. Also, in the case of the tow samples from the Gulf of Aqaba (Eilat), no significant correlation is seen between B/Ca and these other nutrient concentrations, despite a strong correlation with $[PO_4^{3-}]$ (Figure 7). As such, we focus discussion on the specific case of phosphate ion, and the possible mechanisms behind the observed correlation.

One possible explanation is that $[PO_4^{3-}]$ is linked to some other hydrographic factor that influences boron incorporation, but that was not considered in our regression models. For example, areas of high $[PO_4^{3-}]$ conditions are often associated with seasonal upwelling or deep mixing, and typically have higher levels of primary productivity (although we note that this relationship is not always straightforward; *Moore et al*. [2013]). A more plentiful food supply in these areas may result in higher growth rates, and this in turn might influence boron incorporation into foraminiferal calcite via some precipitation rate-dependency [see *Gabitov et al*., 2014; *Uchikawa et al*., 2015]. This suggestion is consistent with the observation that foraminifera fed every day in culture have higher B/Ca than those grown in the open ocean at comparable pH (this study; Figures 4 and 5). However, the extent to which growth and metabolic rates may be linked to crystallographic precipitation rate is unclear. From the perspective of microenvironment alteration [see *Zeebe et al*., 1999], higher food supply in areas of high $[PO_4^{3-}]$ could enhance symbiont activity through fertilization of the microenvironment [*Erez et al*., 1991]. On the other hand, higher food supply might act to acidify the foraminiferal microenvironment via release of more respired CO_2 (which should have opposing effects on B/Ca ratios). Light attenuation is also greater in areas of higher productivity, which should weaken the buffering effect of photosynthetic symbionts in the microenvironment of *G. ruber*, and again should result in lower $\frac{B(OH)_4^-}{DIC}$ (and therefore B/Ca) in these high productivity (high $[PO_4^{3-}]$) regions if light levels influence B/Ca, as proposed by *Babila et al*. [2014]. Finally, if $[PO_4^{3-}]$ in our data set simply reflects productivity, one might expect a similar degree of correlation with other nutrients (such as nitrates), which is not seen.

A second possibility is that the observed correlation between B/Ca and $[PO_4^{3-}]$ is a result of an influence of $[PO_4^{3-}]$ on crystallographic processes. Phosphorous compounds interact with $CaCO_3$ in seawater and are

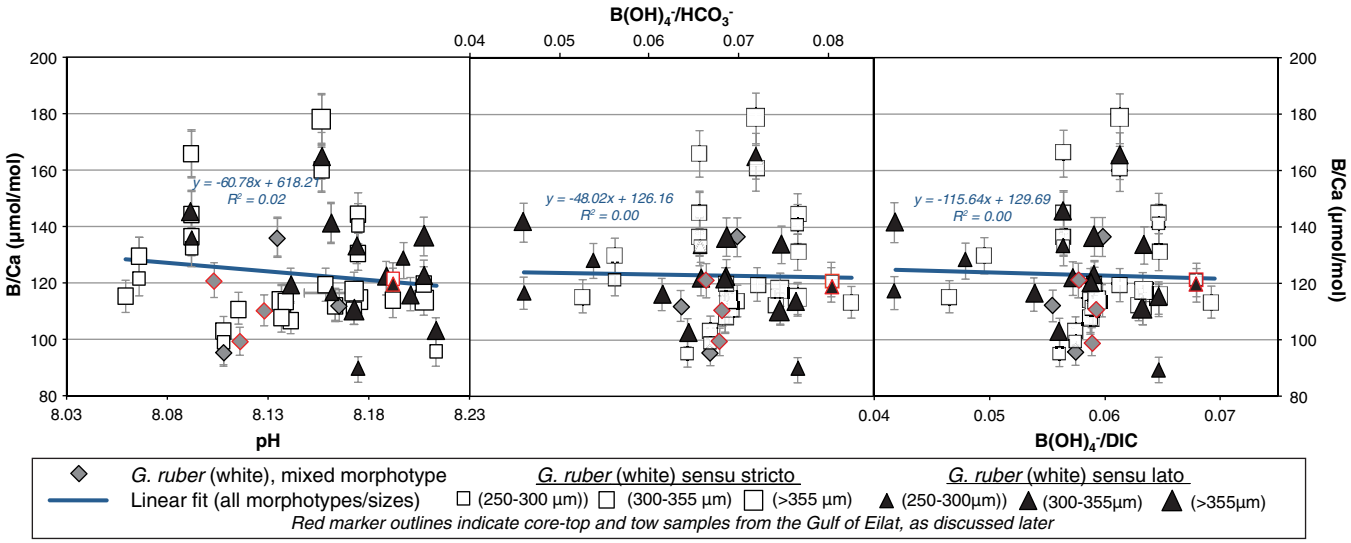

Figure 5. Open-ocean (core-top and sediment trap) *G. ruber* show no correlation between B/Ca and either pH, $\frac{B(OH)_4^-}{HCO_3^-}$ or $\frac{B(OH)_4^-}{DIC}$. Gray diamonds denote mixed morphotype samples, open squares denote sensu stricto, and black triangles denote sensu lato. Error bars are 5% analytical uncertainty (on B/Ca) and 2σ of intra-annual variability in pH at each coretop site.

incorporated into, and adsorbed onto, $CaCO_3$, with incorporation rate dependent on ambient $[PO_4^{3-}]$ [*Berner and Morse*, 1974; *Ishikawa and Ichikuni*, 1981]. Phosphorous compounds have also been known to retard $CaCO_3$ nucleation [*Simkiss*, 1964; *Pytkowicz*, 1973] and precipitation rates [*Reddy*, 1977; *Kitano et al*., 1978b; *Berner et al*., 1978; *Mucci*, 1986; *Burton and Walter*, 1990]. Were the time permitted for the recoordination of tetrahedral boron to trigonal form a limiting factor on the incorporation of boron [as suggested by *Ruiz-Agudo et al*., 2012] retardation of $CaCO_3$ growth by ambient PO_4^{3-} might result in higher B/Ca ratios. More recent experiments, however, suggest a positive correlation between B/Ca and precipitation rate [*Gabitov et al*., 2014]. Alternatively, then, the promotion of amorphous calcium carbonate (ACC) formation by both organic and inorganic PO_4^{3-} [*Dove and Hochella Jr*.,1993; *Bentov et al*., 2010; *Hild et al*., 2008], may allow for greater incorporation of boron, given that ACC will more readily incorporate trace elements [*Bentov and Erez*, 2006; *Cusack and Freer*, 2008].

Kinetics aside, if phosphorous is incorporated into $CaCO_3$ as orthophosphate (PO_4^{3-}) ion, (as supported by *Ishikawa and Ichikuni* [1981] and *Mucci* [1986] but not *Burton and Walter* [1990] or *Lin and Singer* [2006]) then it is possible that paired substitution is required to balance valency, and that boron may be incorporated as a result. For example, two (CO_3^{2-}) ions might substitute for one PO_4^{3-} and one $B(OH)_4^-$ ion. It is also likely that the reorganization of such a large molecule as $[PO_4^{3-}]$ into the carbonate lattice would result in considerable disorder and an increase in the number of kink sites, where boron might more easily be incorporated [*Hemming et al*., 1995].

It is also possible that pH-dependent changes in the speciation of phosphorous (see supporting information Figure S2) in culture experiments towards increasing abundance of orthophosphate ion with increasing pH [*Atlas*, 1975; *Millero*, 1995; *Zeebe and Wolf-Gladrow*, 2001] might at least accentuate apparent carbonate system control, should orthophosphate (PO_4^{3-} ion) be the species incorporated into $CaCO_3$ (as suggested by *Ishikawa and Ichikuni* [1981]). For example, at a fixed total $[P]_{sw}$ (and a temperature of 26°C and salinity of 37.2), the proportion of phosphorous present as orthophosphate ion increases by $>$ 350% (from 6% of total P to 20%) across the range of pH examined here in culture (see Figure 10). Very high concentrations of total $[P]_{sw}$ would be required to explain all of the observed B/Ca variation in culture via alteration of the speciation of aqueous phosphorous and the observed open ocean B/Ca–$[PO_4^{3-}]$ relationship (Figure 10). It is possible, however, that manipulation of culture pH might indirectly produce $[PO_4^{3-}]$-driven changes in B/Ca, whereas in the open ocean (where $[PO_4^{3-}]$ is controlled not only by pH-dependent speciation but also by nutrient cycling and utilization), the correlation between B/Ca and pH (or other carbonate system characterizations) is weakened. *Allen et al*. [2011] cite a mismatch between predicted and observed B/Ca in culture experiments as evidence that "other pH-sensitive ions may be involved in calcification" and suggest an

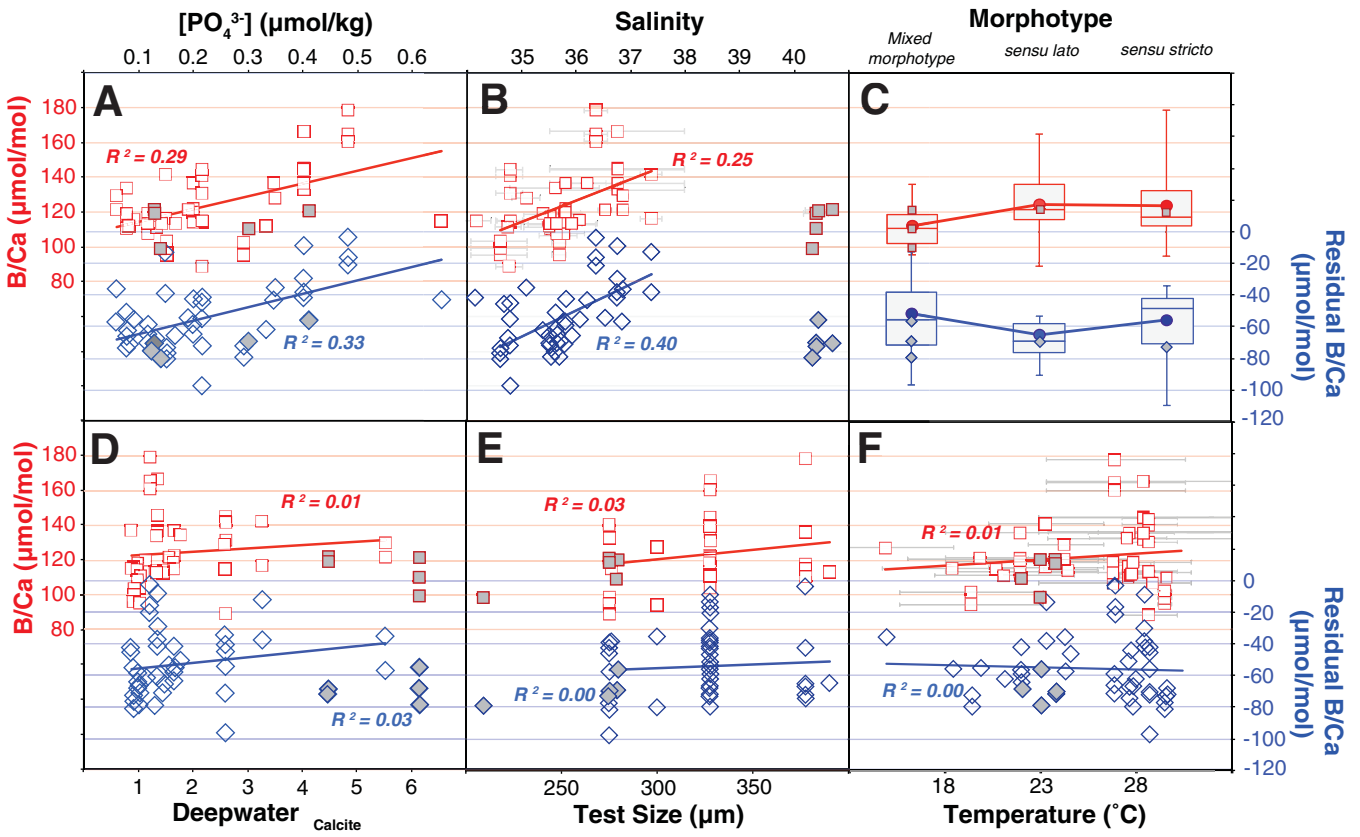

Figure 6. B/Ca ratios (red) and residual B/Ca once the relationship with $\frac{B(OH)_4^-}{DIC}$ seen in culture is removed (blue) in open-ocean specimens of *G. ruber* (white, both morphotypes), compared to $[PO_4^{3-}]$ (a), salinity (b), morphotype (c), bottom water $\Omega_{Calcite}$ (d), test size (e), and temperature (f). Note that despite no significant correlation between B/Ca and $\frac{B(OH)_4^-}{DIC}$ being evident (Figure 4), plotting against the residuals from the relationship seen in culture (i.e., assuming this relationship is reproduced in the open-ocean but is obscured by other controls) often results in improvements in fit. Gulf of Aqaba (Eilat) core-top and tow samples are excluded from regressions (for consistency with multiple regression models), but are plotted in gray. For morphotype, box, and whisker plots illustrate the ranges, interquartile ranges, and median, with the mean values shown as filled circles, and Eilat measurements overlaid in gray. Error bars in Figure 6b and 6f reflect 2 sd of the 12 monthly values from *Takahashi et al.* [2009].

important role for $[CO_3^{2-}]$. While culturing experiments across varying aqueous $[PO_4^{3-}]$ are still required, we propose that PO_4^{3-} may be at least one such pH-sensitive ion influencing boron incorporation.

4.3. The Influence of Salinity on Foraminiferal B/Ca

With the exception of data from the Gulf of Eilat (see section 4.8), open-ocean data presented here support the findings of *Allen et al.* [2011, 2012] that salinity is positively correlated with B/Ca in *G. ruber*, although the slope of this relationship in core-tops seen here ($m = 12.46$) is greater than that seen in cultured *G. ruber* (pink) ($m = 4.5$; *Allen et al.* [2012]). Notably, even when the effect of $\frac{B(OH)_4^-}{DIC}$ from culture is removed from the data and residual B/Ca is tested, salinity remains a significant control: i.e. the effect of salinity is greater than its influence on $\frac{B(OH)_4^-}{DIC}$ alone. This effect of salinity might be partially a result of an increase in $[B]_{sw}$: *Allen et al.* [2011] note that increasing $[B(OH)_4^-]$ by raising total $[B]_{sw}$ at constant pH resulted in a disproportionately large response in B/Ca compared to experiments where $[B(OH)_4^-]$ was increased through pH-dependent speciation. However, *Kitano et al.* [1978a] found that [B] in inorganically precipitated $CaCO_3$ rose with addition of pure NaCl (i.e., with no concurrent rise in $[B]_{sw}$). The mechanism for this is unclear, but it is feasible, for example, that enhanced ionic strength could promote boron adsorption by alteration of the electrokinetic state of the growing crystal surface and the surrounding hydrodynamic boundary layer [*Adamson*, 1982; *Parks*, 1990] to promote adsorption of the negative $B(OH)_4^-$ ion. That said, any such explanation would require a compensating mechanism to explain the low values of B/Ca in the Gulf of Aqaba (Eilat). Note also that while salinity does also have some effect on speciation of aqueous P [*Atlas*, 1975], this effect is negligible over the salinity range studied here.

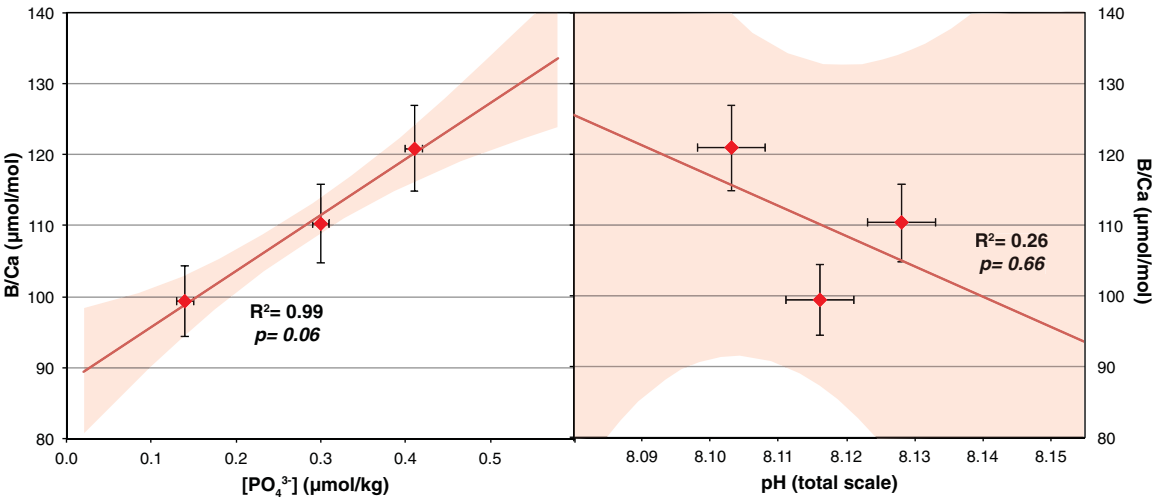

Figure 7. B/Ca ratios in *G. ruber* (mixed morphotype) towed from the Gulf of Aqaba (Eilat) between January and March 2010 correlate strongly with measured $[PO_4^{3-}]$ in surface water sampled at the time of towing, but not with pH (total scale, as calculated from measured DIC and Total Alkalinity). Shaded in red are the regions of 95% confidence for the regression, calculated via 1000 Monte Carlo simulations. Error bars reflect 5% uncertainty on B/Ca measurement, 0.01 µ*M* uncertainty on $[PO_4^{3-}]$ measurement, and 0.005 uncertainty on pH measurement at the UK-OARP carbonate facility.

4.4. No Effect of Temperature on B/Ca Ratios in *G. ruber*

Temperature is not found to be a major control on B/Ca in any of our regression models. This supports observations from cultures of *O. universa* between 18–26°C [*Allen et al*., 2011] and cultures of *G. ruber* and *G. sacculifer* from 24°C to 30°C [*Allen et al*., 2012], as well as observations in open ocean *Neogloboquadrina pachyderma* [*Hendry et al*., 2009] that show no discernible effect of temperature on B/Ca ratios. Therefore, we suggest that observed correlations with temperature in some earlier studies [e.g., *Wara et al*., 2003; *Yu et al*., 2007; *Tripati et al*., 2009] are likely either an artefact of interpreting B/Ca ratios in terms of K_D ($K_D = B/Ca/\frac{B(OH)_4^-}{HCO_3^-}$, as in *Yu et al*. [2007]; *Foster* [2008]; *Tripati et al*. [2009]), which may produce artificial relationships (due to the effect of temperature on the denominator), or alternatively a product of the collinearity of temperature with other hydrographic variables in these sample sets (see *Allen and Hönisch* [2012], for further discussion).

Table 3. Multiple Linear Regression Statistics Output From Core-Top and Sediment Trap *G. ruber*[a]

Factor	Coefficient	Std. Error	*t*	*P*
Intercept	−432.63	104.78	−4.13	1.8×10^{-4}[c]
$[PO_4^{3-}]$	81.91	14.01	5.85	7.72×10^{-7}[c]
Salinity	11.43	2.7	4.23	1.34×10^{-4}[c]
Size	0.17	0.06	2.63	0.01[d]
Deep Ω	4.92	1.95	2.52	0.02[d]
Temperature[b]	0.98	0.59	1.67	0.1
Borate/DIC[b]	707.54	438.53	1.61	0.12
Residuals				
Min.	1st Quart.	Median	3rd Quart	Max.
−25.45	−8.408	−1.171	7.98	26.35
Residual standard error: 12.25 (d.f. = 40)			*F*-statistic: 12.39	
	Multiple R^2: 0.65		Adjusted R^2: 0.60	
$p = 7.73 \times 10^{-8}$				

[a]All sizes and morphotypes included, with the exception of outliers from the Gulf of Eilat.
[b]Note that temperature and $\frac{B(OH)_4^-}{DIC}$ have no significant effect on B/Ca ratios, but they are left in for illustration, and given their inclusion improves the model AIC. Omission of these factors results in no change in the significance of the other factors, nor their relative importance.
[c]Indicates that a factor is a significant contributor to the model to $p < 0.001$.
[d]Indicates $p < 0.05$.

4.5. Deep-Water $\Omega_{Calcite}$: Assessing the Evidence for a Dissolution Effect on B/Ca

While $\Omega_{Calcite}$ at the site of deposition has been shown elsewhere to affect B/Ca ratios in *G. sacculifer* [*Seki et al*., 2010; *Coadic et al*., 2013], it accounts for a very small percentage of the variation seen in core-top *G. ruber* B/Ca presented here (at least within the limited range of $\Omega_{Calcite}$ tested: 0.9–5.2). This lack of a dissolution effect on boron content supports the suggestion that *G. ruber* is a good substrate for the application of boron-based proxies, in agreement with *Seki et al*. [2010]. Apparent resistance to loss of boron via

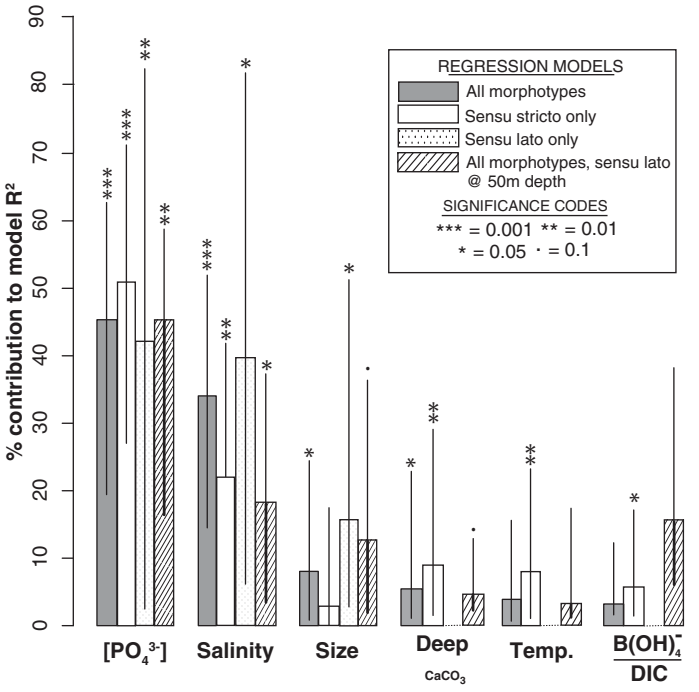

Figure 8. The relative importance of $[PO_4^{3-}]$, salinity, test size, bottom water $\Omega_{Calcite}$, size, temperature, and $\frac{B(OH)_4^-}{DIC}$ as controls on B/Ca variability, across a range of multiple linear regression models. These models are: all morphotypes (in gray), sensu stricto morphotypes only (in white), sensu lato morphotypes only (mottled), and all morphotypes, but assuming a habitat depth of 50 m for *G. ruber* sensu lato (striped). Relative importance is calculated as per *Lindeman et al.* [1980] using the "lmg" method of *Groemping* [2006], using "*R*," with uncertainty on relative importance (at 2σ) determined via 1000 bootstrap subsamples. Note that the *y* axis shows % of overall model R^2 (adjusted) and the metrics are normalized to sum to 100% of this R^2. As in Table 3, *** indicates that a factor is a significant contributor to the model to $p < 0.001$, **indicates significance to $p < 0.01$, * indicates $p < 0.05$, and **dot** indicates significance at only $p < 0.1$. Note that in model fits for *G. ruber* sensu lato only, deepwater $\Omega_{Calcite}$, temperature and $\frac{B(OH)_4^-}{DIC}$ are removed from the model due to their detrimental effects on model AIC [*Akaike*, 1974], and thus are not depicted here.

dissolution could be attributable to a lack of gametogenic calcite in *G. ruber* [*Caron et al.*, 1990], and thus relative homogeneity of test boron concentrations compared to *G. sacculifer*, although we are not aware of any published investigations into intratest variability of B/Ca in *G. ruber* (in contrast to *G. sacculifer; Allen et al.* [2012]). However, since dissolution upon deposition is controlled not only by the saturation state of the waters above sediments, but by processes within the sediment, (such as the supply of organic matter or the degree of bioturbation; see *Peterson and Prell* [1985]; *Schulte and Bard* [2003]; *Hönisch and Hemming* [2004]) an analysis of a mix of core tops (top 0.5–1 cm) and sediment traps such as this cannot fully account for any potential influence of dissolution. As such, the potential for post depositional dissolution effects should still be considered when interpreting down-core records of B/Ca.

4.6. Morphotype Differences in B/Ca Controls

While *G. ruber* sensu lato does not have significantly different B/Ca from sensu stricto at sites where both morphotypes were analyzed (section 3.3, Figure 6c), regression models that incorporate sensu lato tend to exhibit poorer fits. Moreover, salinity appears to be a relatively more powerful control on B/Ca ratios in this group compared to $[PO_4^{3-}]$. This difference in fit is likely the result of either (a) morphospecies-specific variability in boron incorporation or (b) uncertainty in the depth habit of *G. ruber* sensu lato.

While comparisons at core-top sites between sensu stricto and sensu lato reveal no offset, *G. ruber* sensu lato is an umbrella term [from *Wang*, 2000] for what are in reality two genetically distinct subgroups: Type IIa and Type IIb [*Aurahs et al.*, 2011]. In our study, because of sample material limitations, both of these taxa were combined as sensu lato, consequently if these groups exhibit different B/Ca ratios this may result in poorer correlations. Alternatively, it is possible that the poorer fit in *G. ruber* sensu lato is attributable to a difference, or greater variability, in depth habitat in the sensu lato Types IIa and IIb compared to sensu stricto (Type I). Fitting a regression model to sensu lato data with conditions approximated to 50 m depth (supporting information Table S3), and using 50 m depth $[PO_4^{3-}]$ values from WOA [*Garcia et al.*, 2010], improves model fit considerably ($R^2_{(adj.)} = 0.65$ versus 0.53), and increases the importance of $[PO_4^{3-}]$ as the primary control in *G. ruber* sensu lato (Figure 8). Again, testing residual B/Ca (removing the $\frac{B(OH)_4^-}{DIC}$ –B/Ca relationship from culture, using values of $\frac{B(OH)_4^-}{DIC}$ estimated at 50 m) results in even stronger model fits for both sensu lato ($R^2_{(adj.)} = 0.88$) and all *G. ruber* ($R^2_{(adj.)} = 0.70$) data sets when a depth habit of 50 m is assumed for sensu lato (with $[PO_4^{3-}]$ and salinity the significant factors in both cases). Thus it seems likely that differences in regression model fits between these two groups relate more to an uncertainty in assigned depth habitat than any intrinsic differences in boron incorporation between morphotypes, and

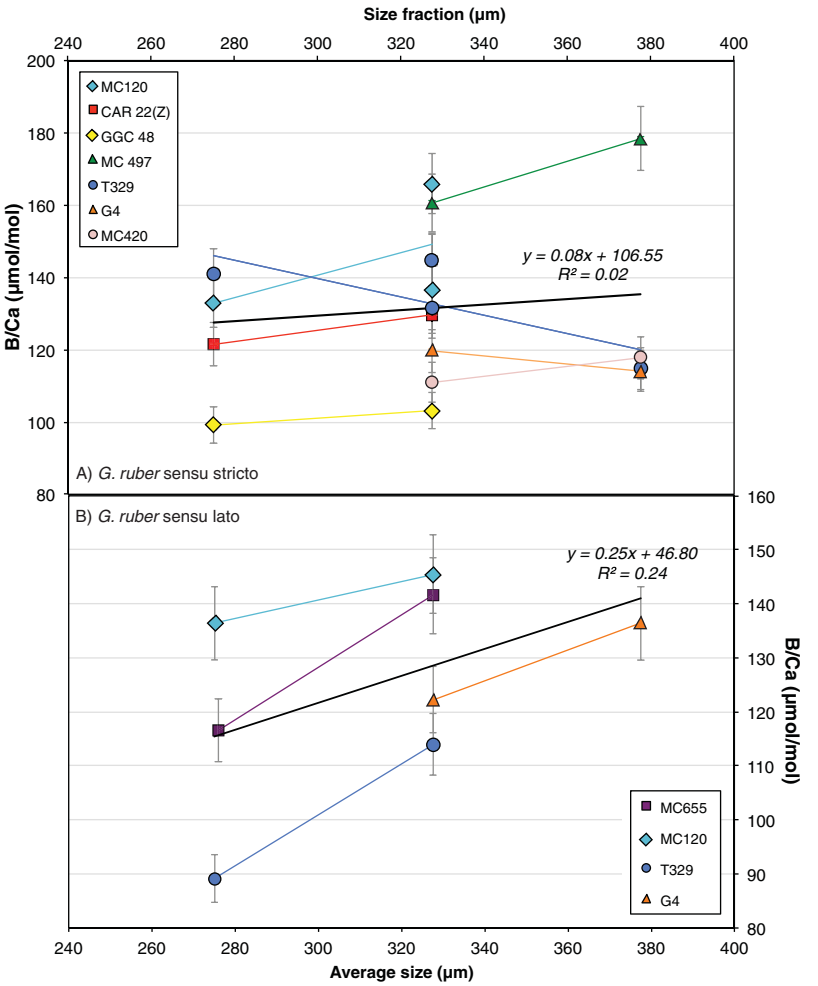

Figure 9. (top)Measured B/Ca ratios across a range of size fractions in *G. ruber* sensu stricto and (bottom)*G. ruber* sensu lato measured from a number of open ocean sample sites. Y-error bars are 5% analytical uncertainty. In each case, a linear regression is plotted through all data (black line). Size fraction is shown as the midrange value sieve fractions 250–300 µm, 300–355 µm, and 355–400 µm.

that greater certainty in the habitat depth in *G. ruber* regionally would improve the goodness-of-fit of the regression models fitted in this study.

4.7. Changes in *G. ruber* B/Ca Ratios with Test Size

Although the contribution of size fraction to the regression model for all morphotypes (Table 3) is statistically significant, this signal is driven only by size-related changes in *G. ruber* sensu lato (or Types IIa and IIb; *Aurahs et al*. [2011]): *Globigerinoides ruber* sensu lato show a marked increase in B/Ca with size ($m = 0.25$, Figure 9; see also supporting information Table S2 and Figure 8), but by contrast in *G. ruber* sensu stricto, no such change in B/Ca is seen ($R^2 = <0.01$, Figure 9; see also supporting information Table S1 and Figure 8). Given that size fraction effects in B/Ca have previously been noted in *G. ruber* [*Ni et al*., 2007], this lack of size fraction effect seen here in *G. ruber* sensu stricto might be considered surprising. However, much of the trend in B/Ca with size observed by *Ni et al*. [2007] is driven by *G. ruber* (pink). In *G. ruber* (white, sensu stricto), apart from lower B/Ca ratios in samples < 250 µm (where morphotype distinction is difficult), values of B/Ca are invariant: *Ni et al*. [2007] observe no trend outside of analytical uncertainty between 280 and 390 µm in diameter. The mechanism by which *G. ruber* sensu lato and *G. ruber* sensu stricto may demonstrate differing trends in B/Ca with size is unclear, but it may result from the differing depth habitats of these groups. If *G. ruber* sensu stricto is limited to surface water throughout its life cycle, but *G. ruber* sensu lato migrates to deeper waters with age (as in *G. sacculifer*; *Erez et al*. [1991]), *G. ruber* sensu lato may experience progressively more elevated $[PO_4^{3-}]$ with depth migration, and hence record progressively higher B/Ca. The lack of any clear size fraction effect in *G. ruber* sensu stricto, meanwhile, may also highlight the

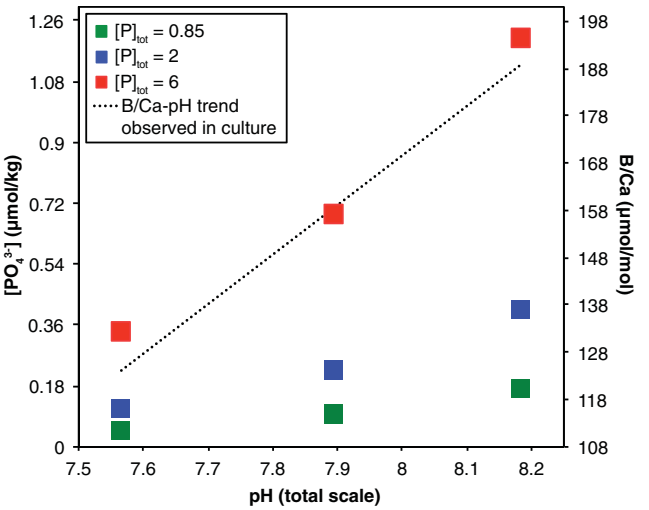

Figure 10. Illustration of pH-dependent change in $[PO_4^{3-}]$ (primary *y* axis) across three concentrations of $[P]_{tot}$. Using the relationship between B/Ca ratios and ambient $[PO_4^{3-}]$ seen in open ocean samples (B/Ca = 72.697*($[PO_4^{3-}]$) + 107.34), this value of $[PO_4^{3-}]$ is used to predict to B/Ca (secondary *y* axis). At sufficiently high concentrations of $[P]_{tot}$, it may be hypothetically possible for pH-dependent speciation of aqueous P to produce the apparent pH trends in B/Ca seen in culture experiments.

lack of a strong carbonate-system control on B/Ca in this species, since increasing $\delta^{11}B$ with size in a subset of these samples [*Henehan et al*., 2013] implies rising microenvironment pH (and thus $\frac{B(OH)_4^-}{DIC}$) with size, and yet no concurrent rise in B/Ca is seen.

4.8. Unusual Conditions in Gulf of Aqaba (Eilat)

As discussed in section 3.3, core-top and tow data from the Gulf of Aqaba (Eilat) were removed from statistical analysis as they were identified as outliers. Salinity in the Gulf of Aqaba (Eilat) is very high ($\geq$40.4), but B/Ca ratios in core-top *G. ruber* from this site are not as elevated as would be expected from the B/Ca-salinity relationships of *Allen et al*. [2012], or from the trends in the other core-top data (Figure 6). Since the experiments of *Allen et al*. [2012] reach salinities comparable to the Gulf of Aqaba (Eilat) and see a rise in B/Ca as a result, lowered ratios seen in Eilat samples are not merely a result of the relationship with salinity being nonlinear. This observation may imply that salinity is not in reality as important a determining factor as our analysis suggests. Indeed, as noted above, the influence of salinity in this data set is $\sim$3$\times$ larger than that observed in culture [*Allen et al*., 2012]. It may be that some unknown correlate with salinity in the open ocean has a significant influence on B incorporation. Without greater constraints on the environmental conditions experienced by open-ocean *G. ruber*, however, we are unable to investigate this further. We note that since tows of *G. ruber* from the Gulf of Aqaba (Eilat) recorded similar B/Ca ratios to specimens from core top sediments in the region, this lower than expected B/Ca is not an artifact of preservation (Table 2). Also, we stress that data from Eilat is not anomalous in terms of the trend of $[PO_4^{3-}]$–B/Ca seen elsewhere (Figure 6).

5. Conclusions

We have examined controls on B/Ca ratios in the planktic foraminifera *G. ruber* from both cultures and globally distributed open-ocean tows, sediment traps and core-top samples. While B/Ca ratios respond strongly to isolated carbonate system manipulation in culture studies, these patterns are not reproduced in the open ocean, and large variations in B/Ca ratios (90–180 µmol/mol) occur within a limited range of ocean pH (8.06–8.21). At best, the influence of pH, $\frac{B(OH)_4^-}{HCO_3^-}$ or $\frac{B(OH)_4^-}{DIC}$ on B/Ca in open-ocean *G. ruber* must be overwhelmed by competing controls, most prominently $[PO_4^{3-}]$ (hitherto unnoted) and salinity (supporting *Allen et al*. [2011, 2012]). That said, anomalous samples from the high salinity Gulf of Aqaba (Eilat) suggest our understanding of B incorporation in $CaCO_3$ is still incomplete.

We observe no discernible influence of temperature on B/Ca ratios. Deep-water $\Omega_{Calcite}$ was not seen to have a strong influence on B/Ca ratios in *G. ruber* within the range of $\Omega_{Calcite}$ studied, suggesting that B/Ca in this taxon is less susceptible to postmortem alteration than in *G. sacculifer*. In addition, no clear size fraction effect was observed in *G. ruber* sensu stricto, despite the change in micro-environment pH (and thus $\frac{B(OH)_4^-}{DIC}$) with size implied by $\delta^{11}B$ [*Henehan et al*., 2013].

While a larger array of open-ocean data and a better constraint on depth habitat in *G. ruber* may help to decipher the competing influences on B/Ca in fossil *G. ruber*, these data urge caution in the interpretation of B/Ca ratios in fossil planktic foraminifera as a palaeocarbonate system proxy.

Acknowledgments

All the data needed to evaluate and replicate this research are supplied in the accompanying tables. In the case of figures that give representative examples of chemical distributions, the data are readily calculable using the constants and conditions supplied in figure captions. The authors first thank Michal Kucera for the provision of core-top material from the archives at the University of Tübingen. From the University of Southampton, we thank the other members of "The B-Team" for their contributions, as well as Matthew Cooper, Agnes Michalik, and Andy Milton for laboratory and technical support and Mark Stinchcombe for nutrient analysis and insight into [PO_4^{3-}] measurement. We thank Barbara Donner (MARUM) for supplying core material to GF from Site GeoB1523-1 and Basak Kısakürek (GEOMAR) for advice and provision of core-top Eilat sample material. M.J.H., K.C.P., and J.W.B.R. thank the students and staff at the IUI Eilat for their assistance during culturing experiments. Jennifer Rutter and Clive Trueman (Southampton) are thanked for statistical assistance, and Gemma Smith and Jack Billinge (Southampton) are thanked for GIS contributions and helpful discussion on the measurement of aqueous PO_4^{3-}, respectively. The manuscript benefitted from the constructive criticism of Jimin Yu, Lennart de Nooijer, and one anonymous reviewer. This work was made possible by a NERC PhD studentship granted to M.J.H., NERC grant NE/D00876X/2 awarded to G.L.F., and ISF grant 551/10 awarded to J.E.

References

Adamson, A. W. (1982), *Physical Chemistry of Surfaces (4th Edition)*, John Wiley & Sons, N. Y.

Akaike, H. (1974), A new look at the statistical model identification, *IEEE Trans. Autom. Control*, *19*(6), 716–723, doi:10.1109/TAC.1974.1100705.

Al-Ammar, A. S., R. K. Gupta, and R. M. Barnes (2000), Elimination of boron memory effect in inductively coupled plasma-mass spectrometry by ammonia gas injection into the spray chamber during analysis, *Spectrochim. Acta Part B At. Spectrosc.*, *55*(6), 629–635, doi:10.1016/S0584-8547(00)00197-X.

Allen, K. A., and B. Hönisch (2012), The planktic foraminiferal B/Ca proxy for seawater carbonate chemistry: A critical evaluation, *Earth Planet. Sci. Lett.*, *345–348*, 203–211, doi:10.1016/j.epsl.2012.06.012.

Allen, K. A., B. Hönisch, S. M. Eggins, J. Yu, H. J. Spero, and H. Elderfield (2011), Controls on boron incorporation in cultured tests of the planktic foraminifer *Orbulina universa*, *Earth Planet. Sci. Lett.*, *309*(3–4), 291–301, doi:10.1016/j.epsl.2011.07.010.

Allen, K. A., B. Hönisch. S. M. Eggins, Y. Rosenthal (2012), Environmental controls on B/Ca in calcite tests of the tropical planktic foraminifer species *Globigerinoides ruber* and *Globigerinoides sacculifer*, *Earth Planet. Sci. Lett.*, *351–352*, 270–280, doi:10.1016/j.epsl.2012.07.004.

Atlas, E. L. (1975) Phosphate Equilibria in Seawater and Interstitial Waters, Ph.D. Thesis. Oregon State Univ. Corvallis, Oreg.

Aurahs, R., Y. Treis, K. Darling, and M. Kucera (2011), A revised taxonomic and phylogenetic concept for the planktonic foraminifer species *Globigerinoides ruber* based on molecular and morphometric evidence, *Mar. Micropaleontol.*, *79*, 1–14, doi:10.1016/j.marmicro.2010.12.001.

Babila, T. L., Y. Rosenthal, and M. H. Conte (2014), Evaluation of the biogeochemical controls on B/Ca of *Globigerinoides ruber* white from the Oceanic Flux Program, Bermuda, *Earth Planet. Sci. Lett.*, *404*, 67–76, doi:10.1016/j.epsl.2014.05.053.

Barker, S., M. Greaves, and H. Elderfield (2003), A study of cleaning procedures used for foraminiferal Mg/Ca paleothermometry, *Geochem., Geophys. Geosyst.*, *4*(9), 8407, doi:10.1029/2003GC000559.

Bentov, S., and J. Erez (2006), Impact of biomineralization processes on the Mg content of foraminiferal shells: A biological perspective, *Geochem. Geophys. Geosys.*, *7*, Q01P08, doi:10.1029/2005GC001015.

Bentov, S., S. Weil, L. Glazer, A. Sagi, and A. Berman (2010), Stabilization of amorphous calcium carbonate by phosphate rich organic matrix proteins and by single phosphoamino acids, *J. Struct. Biol.*, *171*(2), 207–215, doi:10.1016/j.jsb.2010.04.007.

Berner, R. A., and J. W. Morse (1974), Dissolution kinetics of calcium carbonate in sea water; IV, Theory of calcite dissolution, *Am. J. Sci.*, *274*(2), 108–134, doi:10.2475/ajs.274.2.108.

Berner, R. A., J. T. Westrich, R. Graber, J. Smith, and C. S. Martens (1978), Inhibition of aragonite precipitation from supersaturated seawater; a laboratory and field study, *Am. J. Sci.*, *278*(6), 816–837, doi:10.2475/ajs.278.6.816.

Brown, R. E., L. D. Anderson, E. Thomas, and J. C. Zachos (2011), A core-top calibration of B/Ca in the benthic foraminifers *Nuttallides umbonifera* and *Oridorsalis umbonatus*: A proxy for Cenozoic bottom water carbonate saturation, *Earth Planet. Sci. Lett. 310*(3–4), 360–368, doi:10.1016/j.epsl.2011.08.023.

Burton, E. A., and L. M. Walter (1990), The role of pH in phosphate inhibition of calcite and aragonite precipitation rates in seawater, *Geochim. Cosmochim. Acta*, *54*(3), 797–808, doi:10.1016/0016-7037(90)90374-T.

Caron, D. A., R. O. Anderson, J. L. Lindsey, W. W. Faber Jr., and E. Lin Lim (1990), Effects of gametogenesis on test structure and dissolution of some spinose planktonic foraminifera and implications for test preservation, *Mar. Micropaleontol.*, *16*(1–2), 93–116, doi:10.1016/0377–8398(90)90031-G.

Coadic, R., F. Bassinot, E. Douville, E. Michel, D. Dissard, and M. Greaves (2013), A core-top study of dissolution effect on B/Ca in *Globigerinoides sacculifer* from the tropical Atlantic: Potential bias for paleo-reconstruction of seawater carbonate chemistry, *Geochem. Geophys. Geosyst.*, *14*, 1053–1068,doi:10.1029/2012GC004296.

Cook, D. R., and S. Weisberg (1982), *Residuals and Influence in Regression. Monographs on Statistics and Applied Probability*, pp. 10–156, Chapman and Hall, New York.

Cusack, M., and A. Freer (2008), Biomineralization: Elemental and organic influence in carbonate systems, *Chem. Rev.*, *108*, 4433–4454.

de Nooijer, L. J., H. J. Spero, J. Erez, J. Bijma, and G.-J. Reichart (2014), Biomineralization in perforate foraminifera, *Earth Sci. Rev.*, *135*, 48–58, doi:10.1016/j.earscirev.2014.03.013.

Dickson A. G. (1990), Thermodynamics of the dissociation of boric acid in synthetic seawater from 273.15 to 318.15 K, *Deep Sea Res., Part A*, *37*, 755–766, doi:10.1016/0198-0149(90)90004-F.

Dove, P. M., and M. F. Hochella Jr. (1993), Calcite precipitation mechanisms and inhibition by orthophosphate: In situ observations by Scanning Force Microscopy, *Geochim. Cosmochim. Acta*, *57*(3), 705–714, doi:10.1016/0016-7037(93)90381-6.

Erez J. (2003) The source of ions for biomineralization in foraminifera and their implications for paleoceanographic proxies, *Rev. Mineral. Geochem.*, *54*, 115–149, doi:10.2113/0540115.

Erez, J., A. Almogi-Labin, and S. Avraham (1991), On the life history of planktonic foraminifera: lunar reproduction cycle in *Globigerinoides sacculifer* (Brady), *Paleoceanography*, *6*(3), 295–306, doi:10.1029/90PA02731.

Foster, G. L. (2008), Seawater pH, pCO_2 and [CO_3^{2-}] variations in the Caribbean Sea over the last 130kyr: A boron isotope and B/Ca study of planktic foraminifera, *Earth Planet. Sci. Lett.*, *271*(1–4), 254–266, doi:10.1016/j.epsl.2008.04.015.

Gabitov, R. I., C. Rollion-Bard, A. Tripati, and A. Sadekov (2014), In situ study of boron partitioning between calcite and fluid at different crystal growth rates, *Geochim. Cosmochim. Acta*, *137*, 81–92, doi:10.1016/j.gca.2014.04.014.

Garcia, H. E., R. A. Locarnini, T. P. Boyer, J. I. Antonov, M. M. Zweng, O. K. Baranova, and D. R. Johnson (2010), World Ocean Atlas 2009, in *Nutrients (Phosphate, Nitrate, Silicate)*, vol. 4, edited by S. Levitus, NOAA Atlas NESDIS 71. p. 398, U.S. Gov. Print. Off.

Gloor, M., N. Gruber, J. Sarmiento, C. L. Sabine, R. A. Feely, and C. Rödenbeck (2003), A first estimate of present and preindustrial air-sea CO_2 flux patterns based on ocean interior carbon measurements and models, *Geophys. Res. Lett.*, *30*(1), 1010, doi: 10.1029/2002GL015594.

Groemping, U. (2006) Relative importance for linear regression in r: The package *relaimpo*, *J. Stat. Software*, *17*(1), 1–27.

He, M., Y. Xiao, Z. Jin, W. Liu, Y. Ma, Y. Zhang, and C. Luo (2013) Quantification of boron incorporation into synthetic calcite under controlled pH and temperature conditions using a differential solubility technique, *Chem. Geol.*, *337–338*, 67–74, doi:10.1016/j.chemgeo.2012.11.013.

Hemleben, C., M. Spindler, and O. R. Erson (1989), *Modern Planktonic Foraminifera*, Springer, Berlin, 220–257.

Hemming, N. G., and G. N. Hanson (1992), Boron isotopic composition and concentration in modern marine carbonates, *Geochim. Cosmochim. Acta*, *56*(1), 537–543, doi:10.1016/0016-7037(92)90151-8.

Hemming, N. G., R. J. Reeder, and G. N. Hanson (1995), Mineral-fluid partitioning and isotopic fractionation of boron in synthetic calcium carbonate, *Geochim. Cosmochim. Acta*, *59*(2), 371–379, doi:10.1016/0016-7037(95)00288-B.

Hendry, K. R., R. E. M. Rickaby, M. P. Meredith, and H. Elderfield (2009), Controls on stable isotope and trace metal uptake in *Neogloboquadrina pachyderma* (sinistral) from an Antarctic sea-ice environment, *Earth. Planet. Sci. Lett.*, *278*(1–2), 67–77, doi:10.1016/j.epsl.2008.11.026.

Henehan, M. J. et al. (2013), Calibration of the boron isotope proxy in the planktonic foraminifera *Globigerinoides ruber* for use in palaeo-CO_2 reconstruction, *Earth Planet. Sci. Lett.*, *364*, 111–122, doi:10.1016/j.epsl.2012.12.029.

Hesterberg, T., D. S. Moore, S. Monaghan, A. Clipson, and R. Epstein (2005), Bootstrap methods and permutation tests, in *The Practice of Business Statistics*, Chap. 18, edited by D. S. Moore and G. P. McCabe, Freeman, Cooper, N. Y.

Hild, S., O. Marti, and A. Ziegler (2008), Spatial distribution of calcite and amorphous calcium carbonate in the cuticle of the terrestrial crustaceans *Porcellio scaber* and *Armadillidium vulgare*, *J. Struct. Biol.*, *163*(1), 100–108, doi:10.1016/j.jsb.2008.04.010.

Hönisch, B., and N. G. Hemming (2004), Ground-truthing the boron isotope-paleo-pH proxy in planktonic foraminifera shells: Partial dissolution and shell size effects, *Paleoceanography*, *19*, PA4010, doi:200410.1029/2004PA001026.

Ishikawa, M., and M. Ichikuni (1981), Coprecipitation of phosphate with calcite, *Geochem. J.*, *15*, 283–288.

Kakihana, H., M. Kotaka, and S. Satoh (1977), Fundamental studies on the ion-exchange separation of boron isotopics, *Bull. Chem. Soc. Jpn.*, *50*(1), 158–163.

Kawahata, H. (2005), Stable isotopic composition of two morphotypes of *Globigerinoides ruber* (white) in the subtropical gyre in the north pacific, *Paleontol. Res.*, *9*, 27–35, doi:10.2517/prpsj.9.27.

Key, R. M., A. Kozyr, C. L. Sabine, K. Lee, R. Wanninkhof, J. L. Bullister, R. A. Feely, F. J. Millero, C. Mordy, and T. Peng (2004), A global ocean carbon climatology: Results from global data analysis project (GLODAP), *Global Biogeochem. Cycles*, *18*, GB4031, doi:200410.1029/2004GB002247.

Key, R. M., et al. (2010), The CARINA data synthesis project: introduction and overview, *Earth Sys. Sci. Data*, *2*, 105–121.

Kitano, Y., M. Okumura, and M. Idogaki (1978a) Co-precipitation of borate-boron with calcium carbonate, *Geochem. J.*, *12*(3), 183–189.

Kitano, Y., M. Okumura, and M. Idogaki (1978b), Uptake of phosphate ions by calcium carbonate, *Geochem. J.*, *12*(1), 29–37.

Kuroyanagi, A., and H. Kawahata (2004), Vertical distribution of living planktonic foraminifera in the seas around Japan, *Mar. Micropaleontol.*, *53*(1–2), 173–196, doi:10.1016/j.marmicro.2004.06.001.

Lin, Y. P., and P. C. Singer (2006), Inhibition of calcite precipitation by orthophosphate: Speciation and thermodynamic considerations, *Geochim. Cosmochim. Acta*, *70*(10), 2530–2539, doi:10.1016/j.gca.2006.03.002.

Lindeman, R. H., P. F. Merenda, and R. Z. Gold (1980), *Introduction to Bivariate and Multivariate Analysis*, Scott Foresman and Co., Glenview, Ill, 1–444.

Löwemark, L., W. L. Hong, T. F. Yui, and G. W. Hung (2005), A test of different factors influencing the isotopic signal of planktonic foraminifera in surface sediments from the northern South China Sea, *Mar. Micropaleontol.*, *55*(1–2), 49–62, doi:10.1016/j.marmicro.2005.02.004.

Marshall, B. J., R. C. Thunell, M. J. Henehan, Y. Astor, and K. E. Wejnert (2013), Planktonic foraminiferal area density as a proxy for carbonate ion concentration: A calibration study using the Cariaco Basin Ocean time series, *Paleoceanography*, *28*, 363–376, doi:10.1002/palo.20034.

Millero, F. J. (1995), Thermodynamics of the carbon dioxide system in the oceans, *Geochim. Cosmochim. Acta*, *59*(4), 661–677, doi:10.1016/0016–7037(94)00354-O.

Moore, C. M., et al. (2013), Processes and patterns of oceanic nutrient limitation, *Nat. Geosci.*, *6*(9), 701–710, doi:10.1038/ngeo1765.

Mucci, A. (1986), Growth kinetics and composition of magnesian calcite over-growths precipitated from seawater: Quantitative influence of orthophosphate ions, *Geochim. Cosmochim. Acta*, *50*(10), 2255–2265, doi:10.1016/0016–7037(86)90080-3.

Naik, S. S., and P. D. Naidu (2014), Boron/Calcium ratios in *Globigerinoides ruber* from the Arabian Sea: Implications for controls on Boron incorporation. *Marine Micropaleontol.*, *107*, 1–7, doi:10.1016/j.marmicro.2014.01.004.

Nehrke G., N. Keul, G. Langer, L. J. de Nooijer, J. Bijma, and A. Meibom (2013), A new model for biomineralization and trace-element signatures of Foraminifera tests. *Biogeosciences*, *10*, 6759–6767, doi:10.5194/bg-10-6759-2013.

Ni, Y., G. L. Foster, T. Bailey, T. R. Elliott, D. N. Schmidt, P. Pearson, B. Haley, and C. Coath (2007), A core-top assessment of proxies for the ocean carbonate system in surface-dwelling foraminifers, *Paleoceanography*, *22*, PA3212, doi:10.1029/2006PA001337.

Nir, O., A. Vengosh, J. S. Harkness, G. S. Dwyer, and O. Lahav (2015), Direct measurement of the boron isotope fractionation factor: Reducing the uncertainty in reconstructing ocean paleo-pH, *Earth Planet. Sci. Lett.*, *414*, 1–5, doi:10.1016/j.epsl.2015.01.006.

Numberger L., C. Hemleben, R. Hoffmann, A. Mackensen, H. Schulz, J.-M. Wunderlich, and M. Kucera (2009), Habitats, abundance patterns and isotopic signals of morphotypes of the planktonic foraminifer *Globigerinoides ruber* (d'Orbigny) in the eastern Mediterranean Sea since the Marine Isotopic Stage 12, *Mar. Micropaleontol.*, *73*, 90–104, doi:10.1016/j.marmicro.2009.07.004.

Parks, G. A. (1990), Surface energy and adsorption at mineral/water interfaces; an introduction, *Reviews in Mineralogy and Geochemistry*, *23*(1), 133–175.

Palmer, M. R., G. Brummer, M. J. Cooper, H. Elderfield, M. Greaves, G.-J. Reichart, S. Schouten, and J. M. Yu (2010), Multi-proxy reconstruction of surface water pCO_2 in the northern Arabian Sea since 29 ka, *Earth Planet. Sci. Lett.*, *295*(1–2), 49–57, doi:10.1016/j.epsl.2010.03.023.

Paquette, J., and R. J. Reeder (1995), Relationship between surface structure, growth mechanism, and trace element incorporation in calcite, *Geochim. Cosmochim. Acta*, *59*, 735–749, doi:10.1016/0016-7037(95)00004-J.

Peterson, L., and W. Prell (1985), Carbonate dissolution in recent sediments of the eastern equatorial Indian Ocean: Preservation patterns and carbonate loss above the lysocline, *Mar. Geol.*, *64*(3–4), 259–290, doi:10.1016/0025-3227(85)90108-2.

Pytkowicz, R. M. (1973) Calcium carbonate retention in supersaturated seawater, *Am. J. Sci.*, *273*(6), 515–522, doi:10.2475/ajs.273.6.515.

Rae, J. W. B., G. L. Foster, D. N. Schmidt, and T. Elliott (2011), Boron isotopes and B/Ca in benthic foraminifera: Proxies for the deep ocean carbonate system, *Earth Planet. Sci. Lett.*, *302*(3–4), 403–413, doi:10.1016/j.epsl.2010.12.034.

Raitzsch M., E. C. Hathorne, H. Kuhnert, J. Groeneveld, and T. Bickert (2011), Modern and late Pleistocene B/Ca ratios of the benthic foraminifer *Planulina wuellerstorfi* determined with laser ablation ICP-MS, *Geology*, *39*, 1039–1042, doi:10.1130/G32009.1.

Reddy, M. M. (1977), Crystallization of calcium carbonate in the presence of trace concentrations of phosphorus-containing anions: I. Inhibition by phosphate and glycerophosphate ions at pH 8.8 and 25°C. *J. Cryst. Growth*, *41*(2), 287–295, doi:10.1016/0022-0248(77)90057-4.

Ruiz-Agudo, E., C. Putnis, M. Kowacz, M. Ortega-Huertas, and A. Putnis (2012), Boron incorporation into calcite during growth: Implications for the use of boron in carbonates as a pH proxy. *Earth Planet. Sci. Lett.*, *345–348*, 9–17, doi:10.1016/j.epsl.2012.06.032.

Russell, A. D., B. Hönisch, H. J. Spero, and D. W. Lea, (2004), Effects of seawater carbonate ion concentration and temperature on shell U, Mg, and Sr in cultured planktonic foraminifera, *Geochim. Cosmochim. Acta*, *68*(21), 4347–4361, doi:10.1016/j.gca.2004.03.013.

Sanyal, A., N. G. Hemming, W. S. Broecker, D. W. Lea, H. J. Spero, and G. N. Hanson (1996), Oceanic pH control on the boron isotopic composition of foraminifera: Evidence from culture experiments, *Paleoceanography*, *11*(5), 513–517.

Sanyal, A., M. Nugent, R. Reeder, and J. Bijma (2000), Seawater pH control on the boron isotopic composition of calcite: Evidence from inorganic calcite precipitation experiments. *Geochim. Cosmochim. Acta*, *64*(9), 1551–1555, doi: 10.1016/S0016-7037(99)00437-8.

Sanyal, A., J. Bijma, H. J. Spero, and D. W. Lea (2001), Empirical relationship between pH and the boron isotopic composition of *Globigerinoides sacculifer*: Implications for the boron isotope paleo-pH proxy, *Paleoceanography*, *16*(5), 515–519.

Schulte, S., and E. Bard (2003), Past changes in biologically mediated dissolution of calcite above the chemical lysocline recorded in Indian Ocean sediments, *Quat. Sci. Rev.*, *22*(15–17), 1757–1770, doi:10.1016/S0277-3791(03)00172-0.

Seki, O., G. L. Foster, D. N. Schmidt, A. Mackensen, K. Kawamura, and R. D. Pancost (2010), Alkenone and boron-based Pliocene pCO_2 records, *Earth Planet. Sci. Lett.*, *292*(1–2), 201–211, doi:10.1016/j.epsl.2010.01.037.

Simkiss, K. (1964), The inhibitory effects of some metabolites on the precipitation of calcium carbonate from artificial and natural sea water, *J. Cons. Int. Explor. Mer.*, *29*(1), 6–18, doi:10.1093/icesjms/29.1.6.

Steinke, S., H. Chiu, P. Yu, C. Shen, L. Löwemark, H. Mii, and M. Chen (2005), Mg/Ca ratios of two *Globigerinoides ruber* (white) morphotypes: Implications for reconstructing past tropical/subtropical surface water conditions. *Geochem. Geophys. Geosyst.*, *6*, Q11005, doi:10.1029/2005GC000926.

Steinke, S., M. Kienast, J. Groeneveld, L. Lin, M. Chen, and R. Rendle-Bühring (2008), Proxy dependence of the temporal pattern of deglacial warming in the tropical south china sea: Toward resolving seasonality, *Quat. Sci. Rev.*, *27*(7–8), 688–700, doi:10.1016/j.quascirev.2007.12.003.

Takahashi, T., et al. (2009), Climatological mean and decadal change in surface ocean pCO_2, and net sea–air CO_2 flux over the global oceans, *Deep Sea Res., Part. II*, *56*(8), 554–577, doi: 10.1016/j.dsr2.2008.12.009.

Tripati, A. K., C. D. Roberts, and R. A. Eagle (2009), Coupling of CO_2 and ice sheet stability over major climate transitions of the last 20 million years, *Science*, *326*(5958), 1394–1397, doi:10.1126/science.1178296.

Uchikawa, J., D. E. Penman, J. C. Zachos, and R. E. Zeebe (2015), Experimental evidence for kinetic effects on B/Ca in synthetic calcite: Implications for potential B(OH)4− and B(OH)3 incorporation, *Geochim. Cosmochim. Acta*, *150*, 171–191, doi:10.1016/j.gca.2014.11.022.

Van Heuven S., D. Pierrot, J. W. B. Rae, E. Lewis, and D. W. R. Wallace (2011), *MATLAB Program Developed for CO_2 System Calculations.*, Carbon Dioxide Information Analysis Center, Oak Ridge National Laboratory, U.S. [Available at: http://cdiac.ornl.gov/ftp/co2sys/CO2SYS_calc_MATLAB/]

Wang, L. (2000), Isotopic signals in two morphotypes of *Globigerinoides ruber* (white) from the South China Sea: Implications for monsoon climate change during the last glacial cycle, *Palaeogeogr. Palaeoclimatol. Palaeoecol.*, *161*(3–4), 381–394, doi:10.1016/S0031-0182(00)00094-8.

Wara, M. W., M. L. Delaney, T. D. Bullen, and A. C. Ravelo (2003), Possible roles of pH, temperature, and partial dissolution in determining boron concentration and isotopic composition in planktonic foraminifera, *Paleoceanography*, *18*(4), 1100, doi: 10.1029/2002PA000797.

Yu, J., and H. Elderfield (2007), Benthic foraminiferal B/Ca ratios reflect deep water carbonate saturation state, *Earth Planet. Sci. Lett.*, *258*(1–2), 73–86, doi:10.1016/j.epsl.2007.03.025.

Yu, J. M., J. Day, M. J. Greaves, and H. Elderfield (2005), Determination of multiple element/calcium ratios in foraminiferal calcite by quadropole ICP-MS, *Geochem. Geophys. Geosyst.*, *6*, Q08P01, doi:10.1029/2005GC000964.

Yu, J., H. Elderfield, and B. Hönisch (2007), B/Ca in planktonic foraminifera as a proxy for surface seawater pH, *Paleoceanography*, *22*, PA2202, doi:10.1029/2006PA001347.

Yu, J., D. J. R. Thornalley, J. W. B. Rae, and I. N. McCave (2013), Calibration and application of B/Ca, Cd/Ca and $\delta^{11}B$ in *Neogloboquadrina pachyderma* (sinistral) to constrain CO_2 uptake in the subpolar North Atlantic during the last deglaciation, *Paleoceanography*, *28*, 237–252, doi:10.1002/palo.20024.

Zeebe, R. E., and D. A. Wolf-Gladrow (2001), CO_2 in seawater: Equilibrium, kinetics, isotopes, *65 Elsevier Oceanogr. Ser.*, *7*, Elsevier, Amsterdam, 1–84.

Zeebe, R. E., J. Bijma, and D. A. Wolf-Gladrow (1999), A diffusion-reaction model of carbon isotope fractionation in foraminifera, *Mar. Chem.*, *64*(3), 199–227, doi:10.1016/S0304-4203(98)00075-9.